energies

MDPI

Article

Development of a Simple Methodology Using Meteorological Data to Evaluate Concentrating Solar Power Production Capacity

Ailton M. Tavares [1,2], Ricardo Conceição [3], Francisco M. Lopes [4] and Hugo G. Silva [2,5,6,*]

[1] Instituto de Ciências da Terra (ICT), IIFA, Universidade de Évora, Rua Romão Ramalho 59, 7002-554 Évora, Portugal
[2] Laboratório Associado de Energia, Transporte e Aeronáutica (LAETA), Universidade de Évora, Rua Romão Ramalho 59, 7002-554 Évora, Portugal
[3] High Temperature Processes Unit, IMDEA Energy, Avda. Ramón de La Sagra 3, 28935 Móstoles, Madrid, Spain
[4] Instituto Dom Luiz (IDL), Faculdade de Ciências, Universidade de Lisboa, Campo Grande, 1749-016 Lisbon, Portugal
[5] Departamento de Física, ECT, Universidade de Évora, Rua Romão Ramalho 59, 7002-554 Évora, Portugal
[6] INEGI Alentejo, Universidade de Évora, Largo dos Colegiais 2, 7000-803 Évora, Portugal
* Correspondence: hgsilva@uevora.pt; Tel.: +351-967-480-736

Abstract: Evaluation of the Concentrating Solar Power capacity factor is critical to support decision making on possible regional energy investments. For such evaluations, the System Advisor Model is used to perform capacity factor assessments. Among the required data, information concerning direct normal irradiance is fundamental. In this context, the Engerer model is used to estimate direct normal irradiance hourly values out of global horizontal irradiance ground measurements and other observed meteorological variables. Model parameters were calibrated for direct normal irradiance measurements in Évora (Southern Portugal), being then applied to a network of 90 stations, part of the Portuguese Meteorological Service. From the modelled direct normal irradiance, and for stations that comprise 20 years of data, typical meteorological years were determined. Finally, to identify locations of interest for possible installations of Concentrating Solar Power systems, annual direct normal irradiance availabilities and the respective capacity factor, for a predefined power plant using the System Advisor Model, were produced. Results show annual direct normal irradiance availabilities and capacity factors of up to ~2310 kWh/m² and ~36.2% in Castro Marim and in Faro, respectively. Moreover, this study supports energy policies that would promote Concentrating Solar Power investments in Southern Portugal (Alentejo and Algarve regions) and eastern centre Portugal (Beira Interior region), which have capacity factors above 30%.

Keywords: global horizontal irradiance; Engerer model; typical meteorological year; direct normal irradiance mapping; Concentrating Solar Power plant production capacity

Citation: Tavares, A.M.; Conceição, R.; Lopes, F.M.; Silva, H.G. Development of a Simple Methodology Using Meteorological Data to Evaluate Concentrating Solar Power Production Capacity. *Energies* **2022**, *15*, 7693. https://doi.org/10.3390/en15207693

Academic Editor: Juri Belikov

Received: 12 September 2022
Accepted: 3 October 2022
Published: 18 October 2022

1. Introduction

Electricity production from solar power plants is increasingly seen as one of the alternatives to conventional energy production systems. Photovoltaic (PV) systems' contributions to electric power generation have been growing exponentially [1]. Simultaneously, investments towards Concentrating Solar Power (CSP) plants have been increasing in regions where solar resources are suitable for such technology [1]. Although CSP has had a slower growth than PV, it has been widely used [2], with its global installed capacity expected to increase in the near future.

For installation of solar power systems, solar resource characterization is essential. Its assessment consists in solar irradiation availability (kWh/m²) estimation at a given

location considering a long time period [3]. Thus, a long-term database of solar irradiance (W/m^2) is essential to establish: (i) a correct design for an efficient energy conversion; (ii) estimate electricity production; (iii) guarantee the bankability of CSP plants [1,4].

Acquisition of solar irradiance values at the surface can be performed with state-of-the-art instrumentation. For instance, Global Horizontal Irradiance (GHI) is generally measured with pyranometers. In contrast, measurements of Direct Normal Irradiance (DNI) require more equipment, including a sun tracker system where pyrheliometers are assembled. This makes the equipment more costly and regular maintenance necessary [5]. Such limitations constitute a problem for solar system implementation worldwide, not being restricted to the present study region (Portugal). Nonetheless, DNI can be estimated from measured GHI by remote sensed data or using separation models (semi-physical and empirical) for the respective solar components [6,7]. It is worth noting that satellite data accuracy can be affected by clouds and other atmospheric parameters, leading to frequent occurrence of missing data [8]. Since solar concentration systems are highly dependent on DNI, its accurate determination is fundamental [6,9], particularly at sites with significant solar resources in order to maximize solar harvesting. To solve DNI data scarcity, during the last 5 decades, research activity has grown regarding DNI availability estimation from GHI data. In parallel, there has been an increased number of meteorological stations capable of measuring GHI and DNI simultaneously, but most of these are recent (e.g., in Southern Portugal the stations have only roughly 7 years of operation). Therefore, DNI estimations lack statistical significance, which requires at least 15 years of information to have reliable availability estimates [10]. As opposed to these short time series, long-term time series do exist, although these mostly concern GHI.

In depth discussion of DNI estimation from GHI measurements can be found in [6,11]. In particular, in the work of Gueymard and Ruiz-Arias [6], a benchmark test comprising 140 models was performed, in which DNI values from GHI measurements were estimated. Amongst all presented models, the ones that produced the best scores were: the Engerer [12], Perez [13], and Hollands [14] models. Gueymard and Ruiz-Arias [6] tested and validated the Engerer model (Engerer2, henceforth), using high-quality 1 min data of GHI and DNI at 54 research-class stations distributed in seven continents, which were then grouped into in four distinct climate zones: arid, temperate, tropical, and high-albedo. In that study, the best results were found through Engerer2, since it showed consistent DNI estimations for almost all types of climates; it was called a ''quasi-universal" 1 min separation model. According to Gueymard and Ruiz-Arias [6] and Starke [15], the success of Engerer2 is due to the fact that it was derived from 1 min data, hence allowing to predict fast transient phenomena, such as cloud enhancement. In the study by Kim et al. [1], Engerer2 was used as a deterministic prediction model to estimate DNI for the Korean peninsula at three ground stations (namely in Seoul, Buan, and Jeju), being then validated with observational data. Bright and Engerer [16] used Engerer2 to estimate DNI at different time resolutions (at 1, 5, 10, and 30 min), and also at 1 h and 1-day frequencies, which were under five main Köppen–Geiger climate classifications (polar, cold, temperate, arid, and equatorial). The authors used a deterministic clear-sky model to make the original model easy to use, where the clear-sky values were determined using the REST2 model [17]. Results showed good performances carried out by the model for most time resolutions (with the exception of the daily outputs), and for most climate types (except polar). Recently, Dazhi Yang [18] conducted a comprehensive and comparative evaluation of 10 recent separation models, namely, Engerer2 and Engerer4 [12], Starke1 and Starke2 [15], Starke3 [19], Abreu [20], Paulescu [21], Every1 and Every2 [22], and Yang4 [23]. Yang claims that the Yang4 model has the best overall performance, and therefore should replace Engerer2 as the new quasi-universal model [18]. Nevertheless, considering that Engerer2 has been validated in numerous studies, this model is chosen to be used as the basis model of the present work to estimate DNI from GHI, as it presents good scores along with a simple implementation methodology. It is also worth noting that

Engerer2 is also considered due to its deterministic nature, and can be simply implemented worldwide.

The proposed methodology has the potential to be applied in high solar radiation regions of the globe. This study is centred on Portugal due to the exceptional conditions that the country offers for solar power harvesting. Moreover, it is expected to have an important role in solar energy projects in Europe. Mainland Portugal is seen as one of the top candidates to receive such investments [24]. An increase of installed solar power between ~8.1 and 9.9 GW is expected by 2030, corresponding to about 22–27% of the national annual electricity generation [8]. The present work provides a contribution to improve energy management of solar power systems, by developing reliable DNI availability maps for mainland Portugal. To achieve the proposed objective, a 20-year time series of meteorological data is used (including GHI, air temperature, relative air humidity, wind speed, atmospheric pressure, and precipitation), being measured through 90 ground stations, scattered across the country, as part of the *Instituto Português do Mar e da Atmosfera* (IPMA—the Portuguese national meteorological service) network. From the available data, DNI estimations based on Engerer2 [12] are performed for all stations. For the modelled DNI time series, data post-processing is performed, using multivariable regression coefficients to determine new and more accurate datasets. Engerer2 parameters and regression coefficients are then calibrated using DNI data measurements in Évora (reference station) along with other meteorological datasets. The post-processing model is based on the Multivariate Regression Model (MRM) implemented by Lopes et al. [25], which allows to adjust DNI predictions, provided by the European Centre for Medium-Range Weather Forecasts (ECMWF), to ground observations. Additionally, calculation of typical meteorological years (TMY) is performed with the aim of providing representative data of a given region considering a longer period, which is a key step for elaboration of projects of such dimensions [26–28]. To achieve a better assessment regarding CSP plant performance, investors need to have reliable and realistic climate and soiling [29] data to guarantee project viability. Therefore, TMY calculation is very useful, as it carries weather information for an entire year, consisting of representative months of regional climate over a long period of time [27,28]. The method described by Hall et al. [28], examines nine meteorological parameters such as daily means, maximum and minimum values of air and dew point temperatures, daily means and maximum values of wind speed, and daily values of GHI. The method is applied to compute the TMY for mainland Portugal, and, consequently, the mapping of annual DNI availabilities. Finally, the analysis is then focused on capacity factor (CF) mapping performed across the country with the goal of identifying the most suitable locations for the installation of CSP plants. CF outputs can be used as a comparative measure of the amount of energy produced by a power plant during one year to the energy that would be produced if the power plant was operated at nominal power during the same period [30]. The CF has the advantage of revealing the production capacity of a given power plant, regardless of its size. Moreover, to compute CF values, a freely available power plant model is used, namely the System Advisor Model (SAM), from the National Renewable Energy Laboratory, [31]. With the SAM, the user is able to set up a predefined power station, with a very detailed configuration that allows the simulated power to be close to actual operational plants, such as the Andasol3 power plant [32].

The presented work aims to fill the existing gap between solar assessment research and decision making on possible CSP plants by developing a simple and self-contained methodology that can translate common meteorological time series into a figure of merit of CSP plants that can be decisive for their implementation; CF was selected as figure of merit. To the authors' best knowledge, this is the first time that such a methodology has been developed, and it has enabled the earliest estimation of CF values for mainland Portugal. This procedure has led to the identification of three regions that possess high potential for CSP implementations: Alentejo and Algarve (Southern Portugal), and Beira Interior (Eastern Central Portugal). Furthermore, the most important aspect of this

methodology is that it can be applied in a simple way to other regions in the world that possess high potential for CSP. Therefore, this work is considered as a contribution to the implementation of state-of-the-art power plants not only for Portugal, but for the world.

Considering the aforementioned aspects, this manuscript is organized as follows: in Section 2, the work methodology is presented; Section 3, focuses on the results and respective discussion; in Section 4, some implications at a decision making level are drawn for Portugal; lastly, Section 5 summarizes the main conclusions; additional information is added in Appendices A and B.

2. Methodology

2.1. Measurements

A 20-year period of GHI time series is considered in this work (from 2000 to 2019), being continuously measured over 90 weather stations from the IPMA network, scattered across mainland Portugal (Figure 1), providing coverage of the entire country. Regarding the 90 stations shown in Figure 1, 17 are considered main stations (blue squares), while the remaining stations are used as secondary stations (red circles) and the reference station from *Instituto de Ciências da Terra* (ICT—Institute for Earth Sciences) (green diamond), located in Évora city, is also presented. Main stations are those at which hourly observations are made, or at least three times per day, while at secondary stations, at least one observation is performed per day [33]. More details concerning all stations used can be found in Table A1 (Appendix A).

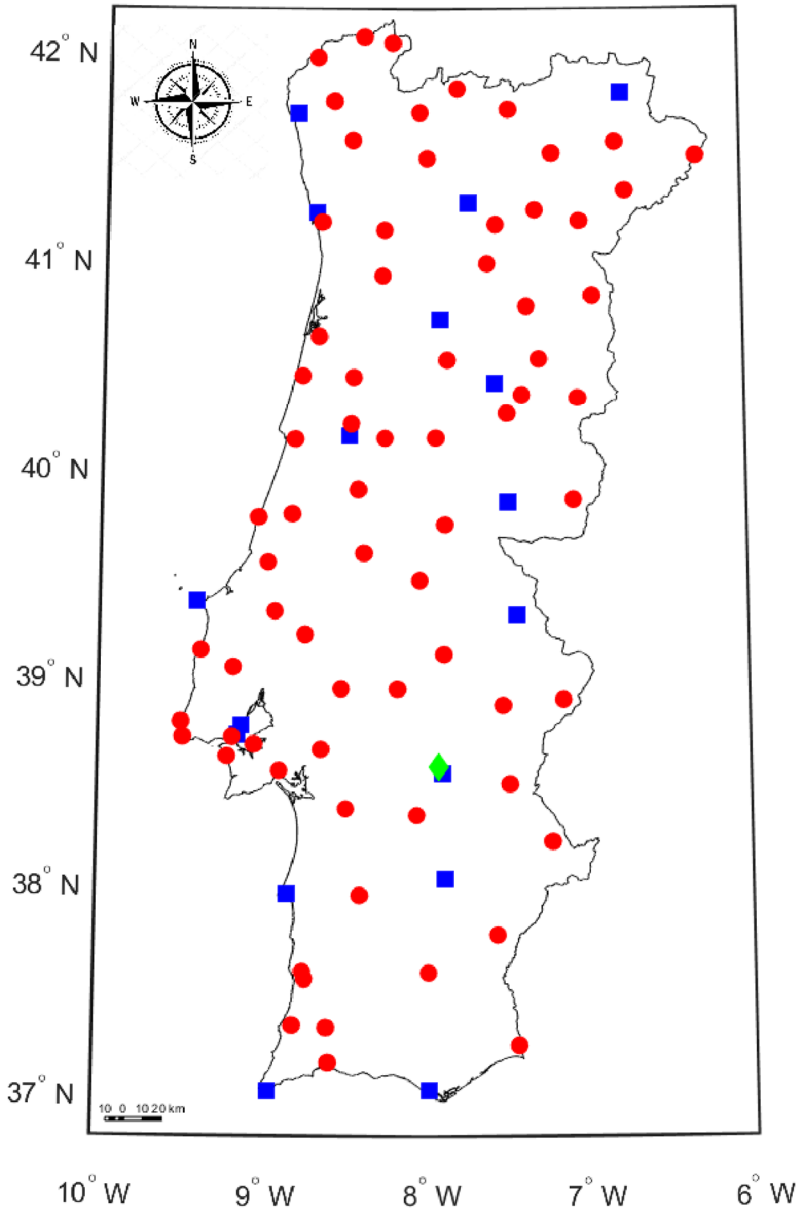

Figure 1. Geographical location of the 90 IPMA ground stations used for GHI measurements in mainland Portugal, considering a 20-year period (from 2000 to 2019). Blue squares represent the main stations, red circles the secondary stations, and the green diamond is the reference station from Instituto de Ciências da Terra (ICT), located in Évora city.

Measurements of GHI were performed in 1 h intervals using state-of-the-art instrumentation, with Kipp&Zonen instrumentation, The Netherlands (www.kippzonen.com/, accessed on 2 October 2022), namely the CM11 and Hukseflux LP02 pyranometers, with the CM11 model being used in the majority of IPMA's stations. Both pyranometers are secondary standard instruments according to the International Organization of Standardization (ISO) 9060:1990 [34]. However, there is no detailed information regarding their calibration and maintenance, due to the large number of stations and their spatial distribution. Thus, in some cases, measurements may be affected by lack of calibration, malfunction, or, more commonly, soiling effect [35,36]. GHI and Diffuse Horizontal Irradiance (DHI) measurements at the reference station in the ICT observatory (University of Évora) were performed with pyranometers (model CMP11), secondary class instrument [34]. DHI was measured using a pyranometer with a shading ball that blocks the beam radiation. For DNI measurements, pyrheliometers were used,

particularly with the model CHP1, a World Meteorological Organization (WMO) first class instrument with an estimated uncertainty on a daily basis of <1% [37]. The instruments used were mounted on a SOLYS2 Sun-Tracker (Kipp&Zonen) [25].

Regarding other meteorological variables measured at IPMA's stations, the air temperature and relative air humidity were recorded at a height of 1.5 m, from which the corresponding hourly averages are used for the analysis; while wind speed is recorded at a height of 10 m, in which the averages of the last 10 min of each hour were used [38]. Air temperature and relative humidity measurements were made with the Vaisala HMP45 sensor, whereas wind speed was measured with the Vaisala WAA 15A anemometer [39].

2.2. Data Pre-Processing

To use reliable data, a prior quality control procedure was performed for all the available measuring stations from IPMA's network, as well as the ICT station. All data points that do not follow the proposed filters (filters for DNI and DHI were only applied to data from the ICT reference station, in which these variables were available), as described in [6], were rejected:

1. $Z < 85°$;
2. $GHI > 0$, $DHI > 0$, $DNI \geq 0$;
3. $DNI < 1100 + 0.03 \times Elev$;
4. $DNI < E_{0n}$;
5. $DHI < 0.95 \times E_{0n} \times \cos^{1.2} Z + 50$;
6. $GHI < 1.50 \times E_{0n} \times \cos^{1.2} Z + 100$;
7. $DHI/GHI < 1.05$ for $GHI > 50$ and $Z < 75°$;
8. $DHI/GHI < 1.10$ for $GHI > 50$ and $Z > 75°$.

In these conditions, "Elev" is the elevation of each station (Table A1), and "E_{0n}" is the irradiance at the top of the atmosphere. Irradiance values below a solar zenith angle (Z) of 85° are considered in this analysis, thus eliminating situations of low irradiance that are not relevant for solar applications, as well as situations where the model has reduced precision (condition 1), mainly due to the high zenith angles: $\cos(Z) \approx 0$. Only positive values of GHI, DHI, and DNI are used (condition 2). DNI values below a certain reference value accounting for station elevation (condition 3) are considered [6]. GHI, DHI, and DNI values below the threshold regarding maximum limits of the baseline surface radiation network (BSRN) [40] (conditions 4, 5, and 6) are also used. Both "Z" and "E_{0n}" were calculated based on the formula proposed by [41], i.e., Equations (2.12) and (2.77), respectively. Following the application of proposed filters on the observed ICT data, the remaining data (which correspond to about 99.32% of the total data) were used to calibrate the corresponding Engerer model parameters, as discussed further on.

2.3. Engerer Model Application

The Engerer2 [12] is a deterministic prediction model, in which the diffuse fraction (K) can be calculated using five predictors, namely: GHI clearness index (k_t), apparent solar time (AST), zenith angle (Z), variability index (k_e), and the deviation (Δk_{tc}) between the observed value of k_t at the surface, and the one obtained under a clear sky (k_{tc}). The following relation between predictors allows one to obtain K:

$$K = \frac{DHI}{GHI}, \tag{1}$$

$$K = C + \frac{1-C}{1+\exp(\beta_0+\beta_1 \times k_t+\beta_2 \times AST+\beta_3 \times Z+\beta_4 \times \Delta k_{tc})} + \beta_5 \times k_e, \tag{2}$$

where C is the value of lower asymptote and β_n (n = 0, …, 5) is the nth Engerer coefficient, whereas Δk_{tc} is given by:

$$\Delta k_{tc} = k_t - k_{tc}, \tag{3}$$

In which k_{tc} is calculated as follows:

$$k_{tc} = \frac{GHI_{cs}}{E_{0n} \times \cos(Z)}. \quad (4)$$

Here, GHI_{cs} is the global horizontal irradiance under clear-sky conditions, and in this study it is defined deterministically as [16]:

$$GHI_{cs} = DNI_{cs} \times \cos(Z) + c \times DNI_{cs}, \quad (5)$$

where DNI_{cs} is the direct normal irradiance under clear-sky conditions, defined as [16]:

$$DNI_{cs} = A \times \exp\left[\frac{-k}{\cos(Z)}\right], \quad (6)$$

in which the coefficients A, k, and c depend on days of the year (d). These coefficients are calculated as follows:

$$\begin{aligned} A &= 1160 + 75 \sin\left[\frac{360(d-275)}{365}\right], \\ k &= 0.174 + 0.035 \sin\left[\frac{360(d-100)}{365}\right], \\ c &= 0.095 + 0.04 \sin\left[\frac{360(d-275)}{365}\right]. \end{aligned} \quad (7)$$

The term k_e is the portion of K attributed in the case of cloud enhancement, defined as:

$$k_e = \max\left(0;\ 1 - \frac{GHI_{cs}}{GHI}\right). \quad (8)$$

Since Engerer2 is made for 1 min temporal resolution, and the fact that GHI data from IPMA's network are measured at 1 h resolution, this work makes use of the Engerer2 model configured for hourly irradiance values of GHI. As previously mentioned, Bright and Engerer [16] evaluated the performance of the Engerer2 model over various time scales, revealing good results for hourly data.

2.4. Data Post-Processing

To reduce the difference between the modelled and observed DNI, post-processing is performed for the modeled data. In this context, a multivariate regression model (MRM) is used to adjust hourly modelled DNI to the observations. The MRM model [25] uses an interactive stepwise function, with an adjusted r-squared criterion, to improve DNI predictions. The method allows to perform all possible combinations between predictors, until the best fitting option is found. In this work, a third-degree polynomial was used to calibrate regression coefficients for three years of measured DNI. The predictors used are the following: modelled DNI (DNI_i^{MOD}), GHI (GHI_i^{OBS}), clear-sky GHI (GHI_i^{CS}) and DNI (DNI_i^{CS}), air temperature (Ta_i^{OBS}), air relative humidity (RH_i^{OBS}), wind speed (WS_i^{OBS}), atmospheric pressure (P_i^{OBS}), and precipitation ($Prec_i^{OBS}$). Thus, a function is used to adjust the modelled DNI (DNI_i^{ADJ}) at hour i according to:

$$DNI_i^{ADJ} = F(DNI_i^{MOD}, GHI_i^{OBS}, GHI_i^{CS}, DNI_i^{CS}, Ta_i^{OBS}, RH_i^{OBS}, WS_i^{OBS}, P_i^{OBS}, Prec_i^{OBS}), \quad (9)$$

where F is adjusted to reduce the error between the DNI_i^{ADJ} and the observed DNI (DNI_i^{OBS}) values. The function F is then applied to all stations under study.

Finally, the post-processing DNI outputs are filtered for: (i) values greater than 1042 W/m² (i.e., the maximum value observed at Évora station), which are replaced by the corresponding clear-sky DNI value at that moment; (ii) negative values, which are replaced by values of modelled DNIs prior to the post-processing. It is worth noting that the parameters calibrated with the observed DNI data in Évora will be used to post-process the modelled DNI in all stations of the IPMA's network.

2.5. Data Gap Filling

Due to equipment malfunction, data gaps in time series are common, particularly for the case of solar radiation measurements. Therefore, gap filling methods are often used, such as the one followed here, in reference to works [3,42]. For data gaps of one or two hours of missing GHI values in a day, missing values are filled by linear interpolation from the non-missing values. For missing periods of three and more hours in a day, a geographical interpolation is performed. The algorithm starts to select the four closest neighbouring stations (k) of the station to which data gaps will be filled (j), and determines the long-term linear regression coefficients (slope and interception point) between this station and the neighbouring ones, as follows:

$$GHI_j = m_{jk} \times GHI_k + b_{jk}, k = 1 \dots 4, \quad (10)$$

With this set of four relations, hourly data gaps in station j are filled by the median of the four hourly values of the measured values on the k stations, GHI_k, on the corresponding hours of the missing data in GHI_j. To obtain reliable data from the linear regression coefficients, outliers are rejected from the correlation by applying the following restrictions: $GHI_j > m_{jk} \times GHI_k + b_{jk} + 2\sigma_{jk}^{+}$ and $GHI_j < m_{jk} \times GHI_k + b_{jk} - 2\sigma_{jk}^{-}$. The parameters σ_{jk}^{+} and σ_{jk}^{-} are the standard deviations calculated from differences for every hour l, as given by:

$$\delta_{jk}(l) = GHI_j(l) - \left[m_{jk} \times GHI_k(l) + b_{jk}\right], \quad (11)$$

where δ_{jk}^{+} means positive differences and δ_{jk}^{-} negative differences, through the following relation [3]:

$$\sigma_{jk}^{\pm} = \sqrt{\frac{\sum_l \left|\delta_{jk}^{\pm}(l)\right|^2}{N-1}}, \quad (12)$$

where N is the number of hours with mutually available data for stations j and k.

After removing the outliers, new values of m_{jk} and b_{jk} are then calculated for the neighbouring stations, while the GHI_j is calculated through Equation (10). For instance, for the station located at Évora, the four closest neighbouring stations are Viana do Alentejo (~26.6 km), Reguengos (~36.6 km), Estremoz (~48.7 km), and Avis (~50.9 km), where the values of m were approximately 1.13, 1.10, 0.98, and 1.12 W/m^2, and the values of b were 3.27, 6.27, 9.00, and 11.69 W/m^2 for the respective stations. The fact that $m \sim 1$ means that the data in the different stations have a similar trend, while b < 12 W/m^2 means that a small deviation exists. This demonstrates the suitability of the adopted interpolation method. Similar results are observed for the other stations of the IPMA's network.

It is noted that regarding the TMY calculation, gap filling was only performed for months that had gaps smaller than five days. Therefore, months with more than five days of missing data were not considered for analysis.

2.6. Typical Meteorological Year Calculation

According to the method proposed in Hall [28], a TMY can be calculated by concatenating twelve typical meteorological months (TMM). The selection of the TMM of each calendar month is calculated based on Finkelstein–Schafer (FS) daily values [43]. Selection is made by comparing cumulative frequency distribution functions (CDFs) of each parameter: mean, maximum and minimum daily value of air temperature, relative humidity, maximum and mean daily values of the wind speed, and daily global horizontal solar irradiation availability, for every month of every year to their long-term distribution. Comprehensive details for this method can be found in [28]. Following these aspects, characteristic annual GHI and DNI availabilities (kWh/m^2/year) are calculated from the summation of hourly irradiance values of TMY regarding each station.

2.7. The Power Plant Model

The power plant simulator, i.e., the SAM, is a freely available financial and performance model designed to facilitate decision making in renewable energy system projects. The model not only allows to make performance predictions, but also energy cost estimates that these systems require [31]. The SAM is used here to simulate a power plant and to estimate its production capacity from meteorological data belonging to IPMA's network. Since there are no DNI measurements in this network, DNI was estimated as previously explained. TMY is elaborated from that meteorological data and SAM simulations are performed using the TMY calculated for each station under study.

In this work, a case study is considered focusing an operational CSP facility with similar configurations to Andasol3, based on the model previously developed on [30,44]. The Andasol3 is a commercial power plant that uses a linear focus parabolic trough system that runs with thermal oil as heat transfer fluid and has 7.5 h indirect molten salt storage capacity at full load. Its solar field aperture area is 510,120 m^2, with a nominal capacity of 50 MW_e and an expected power generation of 175 GWh/year. Further information on the configuration of the power plant can be found in [32].

3. Results and Discussion

3.1. DNI Validation and Calibration

To validate and calibrate the parameters from the Engerer2 and MRM models, four years of DNI measurements, ranging from 2016 to 2019, were used together with ground measurements performed at the ICT station. The Engerer2 parameters are determined from a non-linear regression model, where the model is fitted, with the corresponding parameters determined from an iterative procedure. The proposed validation consists in determining the parameters considering three years of measured GHI, which are then used to estimate DNI for the fourth year and compared with DNI observations for that year. The MRM parameters are also calibrated with three years of modelled DNI, clear-sky GHI and DNI, as well as observed GHI, Ta, RH, WS, P, and Prec. It is important to underline the fact that the modelled DNI is part of the predictors, allowing to improve the MRM. The post-processing method reduces the overestimation of the model when GHI values are strongly composed by DHI (that should correspond to very low DNI values of almost zero) and when GHI observations provide values above 1000 W/m^2, in which cases the Engerer2 model has difficulties in estimating DNI accurately. The MRM parameters are used to post-process the estimated DNI for the fourth year, and thus to compare with measured DNI for the same year. For instance, DNIs from 2016, 2017, and 2019 are used to calibrate the model (adjusting the model and MRM parameters to observations), while DNI from 2018 is used to validate the model estimations against the observations of that year. A similar procedure will be carried out for the remaining years.

To compare model estimations against observations, a statistical analysis was performed using conventional metrics, such as the root mean square error (RMSE), the mean bias error (MBE), and the mean absolute error (MAE), as follows:

$$RMSE = \sqrt{MSE} = \sqrt{\frac{1}{n} \times \sum_{j=1}^{n} \left[I(j) - \hat{I}(j) \right]^2}, \quad (13)$$

$$MBE = \frac{1}{n} \times \sum_{j=1}^{n} \left[I(j) - \hat{I}(j) \right], \quad (14)$$

$$MAE = \frac{1}{n} \times \sum_{j=1}^{n} \left| I(j) - \hat{I}(j) \right|, \quad (15)$$

where $I(j)$ and $\hat{I}(j)$ are the observed and modelled value at hour j, respectively, while n is the number of assessed pairs.

In Table 1, a statistical summary between model outputs and observations is provided. The acronyms MOD1 and MOD2 represent the analysis performed without and with the MRM post-processing method, respectively. Regarding the correlation coefficient (r) and the coefficient of determination (R^2), very small differences are observed when

using MOD2 in comparison to MOD1, reaching an improvement of 1 and 2%, respectively, in 2018. MOD2 shows a decrease of 18% in 2016 to 25% in 2018 in relation to MOD1, with respect to RMSE values. Regarding the MBE values, there is a decrease of more than 60 and 97% in 2016 and 2019, respectively, when MOD2 is used instead of MOD1. There is an improvement of over 20% in 2018 when using MOD2 instead of MOD1, regarding MAE values. These error metric values show that MOD2 presents best scores in comparison to MOD1, which makes it useful for the estimation of DNI.

Table 1. Statistical and descriptive analysis summary for the model towards the measurements using standard error metrics for four consecutive years of hourly data: correlation coefficient (r), coefficient of determination (R^2), root mean square error (RMSE), mean bias error (MBE), and mean absolute error (MAE). MOD1 and MOD2 represent the analysis without and with the MRM model, respectively.

	2016		**2017**		**2018**		**2019**	
Error metrics	MOD1	MOD2	MOD1	MOD2	MOD1	MOD2	MOD1	MOD2
r (---)	0.97	0.98	0.97	0.98	0.97	0.98	0.97	0.98
R^2 (---)	0.94	0.95	0.95	0.96	0.94	0.96	0.95	0.96
RMSE (W/m^2)	92.93	76.33	83.45	66.02	93.73	70.45	87.39	66.06
MBE (W/m^2)	−39.36	−15.41	−31.63	−3.45	−36.06	−2.58	−36.69	0.96
MAE (W/m^2)	61.15	50.24	55.26	47.07	59.88	47.85	55.62	44.71

In Figure 2, a comparative analysis between modelled DNI (with MOD2) and observations is shown. Overall, results show good agreement between modelled and observed values. Within the range between 800 and 1000 W/m² of observed DNI, the model tends to underestimate observations. This range of values represents the clear-sky period and clean atmosphere, in which the model has its limitations, since a deterministic clear-sky model is being used instead of one that considers the actual aerosol load. In such circumstances, the observed GHI will be higher than the modelled GHI_{cs}, making k_e different from zero and increasing K, which results in lower DNI. It is also observed that for DNI values lower than ~30 W/m², the model overestimates observations, reaching values of ~730 W/m², i.e., about 24 times higher. This behaviour is commonly found under cloudy conditions, where measured DNI is significantly lower than the model estimates, due to, for instance, the passing of clouds. Under these conditions DNI is reduced to almost zero, while the decrease is not so significant for GHI, because of the increase in DHI (Figure 2d shows a point circled in red as an example). As a result, if GHI measurements under these conditions are used to estimate DNI, such estimations will have the tendency to be higher than the observed ones. Further explanation is provided along with case studies in what follows.

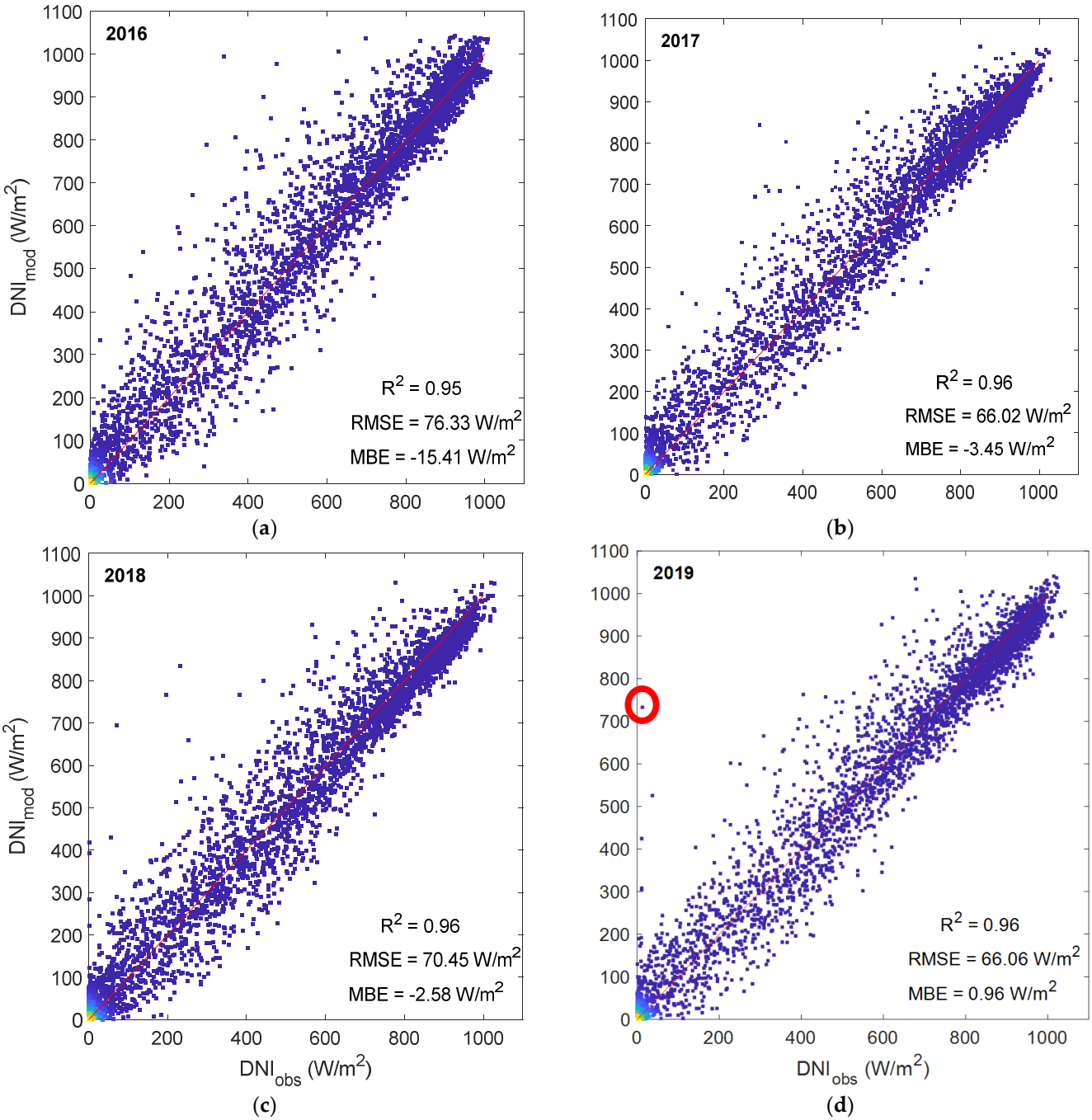

Figure 2. Modelled and observed hourly DNI for: (**a**) 2016, (**b**) 2017, (**c**) 2018, and (**d**) 2019.

The typical daily behaviour for observed DNI and GHI, along with the modelled DNI for 2017 (considered here as a case study), is shown in Figure 3. Four different types of conditions are represented: (a) clear sky, (b) cloudy sky, (c) cloud passage, and (d) several cloud passages. In Figure 3a, it is possible to validate what has been previously reported, i.e., concerning the model behaviour in clear-sky conditions. An underestimation concerning the observations is found, especially near solar noon. In fact, the work conducted in [42] detailed similar behaviour, in which the use of climatologic aerosol values in numerical weather prediction models instead of actual aerosol observations plays an important role. Consequently, for days with a clear and very clean atmosphere, observed DNI will be higher than the one resulting from the model. In the present study, this should stem from the fact that a determinist GHI is being considered for clear sky (GHI_{cs}), which does not consider actual aerosol loads. The use of deterministic GHI for

clear sky is justified by the simplicity and self-containment of the proposed model, enabling an easy application to other regions. In Figure 3b, it can be observed that under cloudy conditions, the model tends to overestimate observations. Similar overestimations are frequently observed in DNI modelling, being extensively discussed in [42]. These values result from the fact that clouds tend to affect more significantly the DNI than the GHI (where DNI reduction is being partially compensated by the DHI increase). Thus, when GHI is used to estimate DNI, the estimation is higher than the actual measured values. This aspect can be observed in Figure 3b for a cloudy day, where at 11 UTC, the observed DNI is ~50 W/m², while the modelled DNI exceeds ~150 W/m². This means that the modelled value is ~3 times higher than the observed in such circumstances. In Figure 3c, the slight increase in the modelled DNI is due to a fast cloud passing that causes the observed DNI to decrease. For the GHI, this effect is not clearly observed since the increase in DHI offsets the GHI value. In Figure 3d, when there are many cloud passages, the model tends to overestimate the observations as depicted by the high values of GHI. Despite these limitations, the modelled DNI follows the observations relatively well.

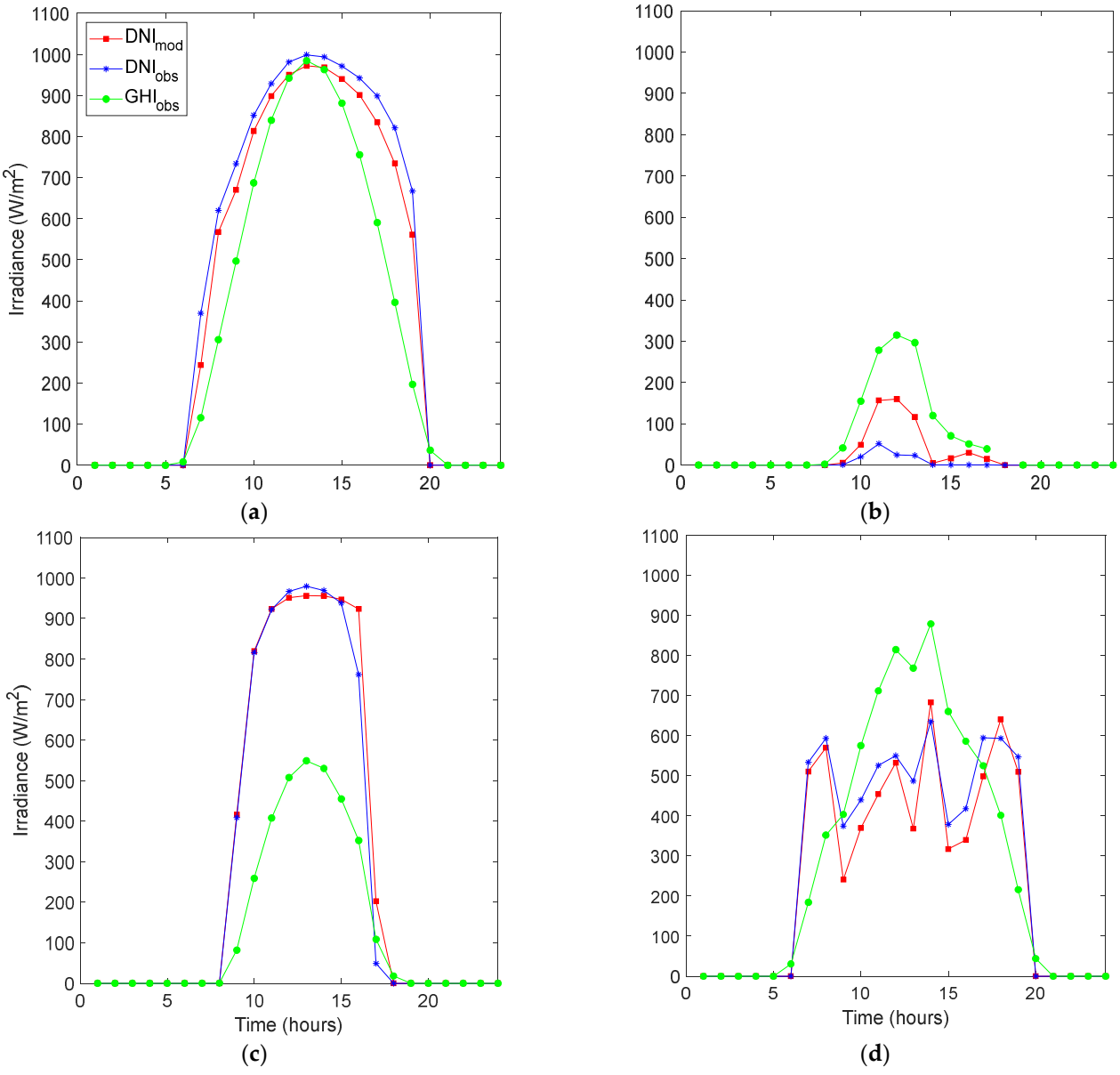

Figure 3. Representation of hourly observed and modelled DNI and observed GHI data: (**a**) clear sky; (**b**) cloudy sky; (**c**) cloud passing; (**d**) several clouds passing. Red square represents model DNI, green circle the observed GHI, and blue asterisk the observed DNI.

Moreover, as previously stated, good correlations between DNI measurements and the model exist for all testing years. Figure 4 shows the probability distribution functions (PDFs) for observed and modelled DNIs, which depict a very similar behaviour. For DNI values in the range between ~920 and ~1000 W/m², the model tends to underestimate the observations. For DNI values in the range between ~800 and ~900 W/m², the model is prone to overestimating the observations, in part due to clouds that affect the observed DNI more than the modelled one, as previously explained. This effect causes the modelled diffuse fraction (K) to decrease while, consequently, the modelled DNI increases more significantly than the observed one. Despite these differences, results show how good the performance of the model is concerning estimating DNI from GHI, thus proving that the adopted method is a reliable source of quality data.

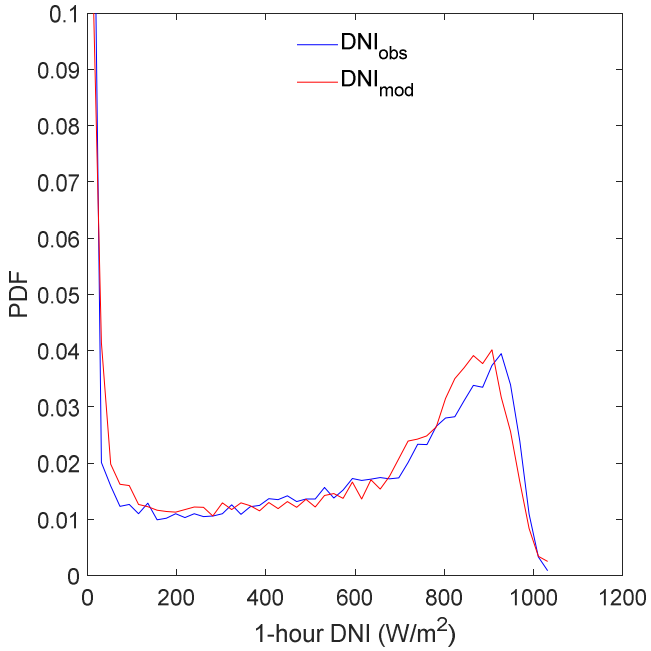

Figure 4. Probability density functions (PDFs) for hourly observed (blue line) and modelled (red line) DNI considering four years (2016 to 2019).

In Table 2, a statistical summary between measurements and model is provided. Results show that the modelled mean values are higher than the observed ones for all years. Regarding the standard deviation, modelled values are smaller than for observations. The DNI annual availability calculated through the model is greater than the observed one for most testing years, except 2019. The highest differences are ~2.93% for 2016, while a minimum of ~0.23% is found for 2019. Regarding the obtained MAE values, on average, the model overestimates or underestimates the observation by ~50.24, 47.07, 47.85, and 44.71 W/m², for 2016, 2017, 2018, and 2019, respectively. On the one hand, these values show the limitations of the adopted model, while on the other hand, in terms of annual availability, these differences are minimal. It is thus expected that the model can provide satisfactory values of direct irradiance availabilities at Évora, and, expectably, at other regions within Portugal.

Table 2. Statistical and descriptive analysis summary for hourly measurements and MOD2 using standard error metrics for four consecutive years (2016–2019) of hourly data: mean, median, standard deviation (σ), DNI availability (E_b), and relative difference of DNI availability (ΔE_b).

	2016		2017		2018		2019	
Error metrics	Obs.	MOD2	Obs.	MOD2	Obs.	MOD2	Obs.	MOD2
Mean (W/m²)	512.91	528.32	549.79	553.24	462.58	465.16	531.38	530.42
Median (W/m²)	585.44	608.17	640.62	651.76	490.28	492.01	608.71	618.10
σ (W/m²)	340.88	340.48	336.46	324.92	341.51	332.86	345.34	337.18
E_b (kWh/m²/year)	2074.36	2135.19	2220.84	2234.65	1862.85	1871.18	2149.16	2144.13
ΔE_b (%)	2.93		0.62		0.45		0.23	

3.2. DNI Estimation

As shown in previous results, 2016 is considered an outlier. Therefore, 3 years (2017, 2018, and 2019) of simultaneous DNI and GHI measurements for Évora are used to perform the calibration of the Engerer2 model parameters. The model parameters, presented in Table 3, show the obtained values in this analysis, as well as the ones obtained from the literature (used for comparison reasons). Despite the differences between obtained and referenced values, which result from the different climatic zones, the parameters lie within reasonable agreement, being thus considered as a validation for the adjusted parameters. It is worth noting that, according to Bright and Engerer [16], no meaningful conclusions can be drawn based on the nature of the parameters alone, as there are some uncertainties related to the (i) clear-sky model and (ii) k_e, which also does not accurately describe situations like cloud enhancement, but rather the relationship of the clear-sky GHI and the measured GHI.

Table 3. Model parameters that result from three years (2017 to 2019) of data measured at the ICT station, in Évora city.

Parameters	Predictor	Present study	Literature
C	-	−0.0861	−0.0097
β_0	-	−3.7884	−5.0317
β_1	k_t	6.8001	8.5084
β_2	AST	0.0050	0.0132
β_3	Z	−0.0003	0.0074
β_4	Δk_{tc}	−1.9639	−3.0329
β_5	k_e	0.0543	0.5640

The calibrated parameters can be used to estimate DNI time series in all stations from IPMA's network, since mainland Portugal's climate can be divided into hot dry summers (Csa), cool dry summers (Csb), and a rainy winter throughout the country, according to the Köppen classification [45].

Finally, post-processing of DNI time series is performed using the MRM parameters calibrated with 3 years (2017, 2018, and 2019) of modelled DNI, GHI, and DNI under clear-sky conditions, and observed *GHI*, T_a, *RH*, *WS*, *P*, and *Prec*, according to Equation (9). Table A2 in Appendix B shows all significant and possible relations between predictors and predictand (terms), the weight (estimates) that each relation has in the respective adjustment, the standard error (SE) obtained, the t-statistics (tStat), and the *p*-value (*p*Value), for DNI hourly adjustment. The coefficients x_1, x_2, x_3, …, x_8 represent, respectively, modelled *DNI* (x_1), observed *GHI* (x_2), *GHI* (x_3), and *DNI* under clear-sky conditions (x_4), and the observed meteorological variables: T_a (x_5), *RH* (x_6), *WS* (x_7), and *P* (x_8). Precipitation revealed negligible weight as predictor.

3.3. TMY Calculation

For the TMY calculation, days with more than 2 h of gaps, and months with more than 5 days of gaps, were rejected. As previously mentioned (Section 2.4), hourly data from the four nearest stations are used to fill the missing periods using the median of data at the same hour for those stations. It is worth noting that the stations of Viana do Castelo, Leiria/Barosa, and Amareleja 2, were removed from the analysis, since these did not have 5 full years of data, thus not having statistical significance. To minimize data loss, the density of the measuring network is such that stations near the ones removed from the analysis can be used as representative of that specific region.

In Figure 5b, the comparison between the PDFs for three years (from 2017 to 2019) of measured (in purple) and modelled DNI (in red and green), and the one calculated from TMY data (in blue), is shown. The PDFs of modelled DNI at the ICT station (in red) and at the IPMA station at Évora (in green) are shown to provide an easy interpretation of the results. For comparison reasons, the PDFs of the GHI observed at the ICT and IPMA stations are plotted along with the GHI found with the TMY (Figure 5a). Between DNI values of ~750 to 950 W/m², the PDF for observed data is higher than that the one from the model (calculated from TMY). It is noticeable that there was the same behaviour in the PDF plotted with the IPMA's DNI data calculated for 2017 to 2019 against the PDF obtained from the DNI observed at the ICT station during the same period. This means that values in this range are found more frequently for observations than the model data from IPMA. This is somehow the inverse behaviour to that found in Figure 4. For DNI values above 950 W/m², the PDFs of the model from IPMA data are higher than the PDF from observation. Again, there is an opposite behaviour to that seen in Figure 4, which leads to the conclusion that these values are directly related to the values of GHI observed at the IPMA station in Évora, as can be seen in Figure 5a.

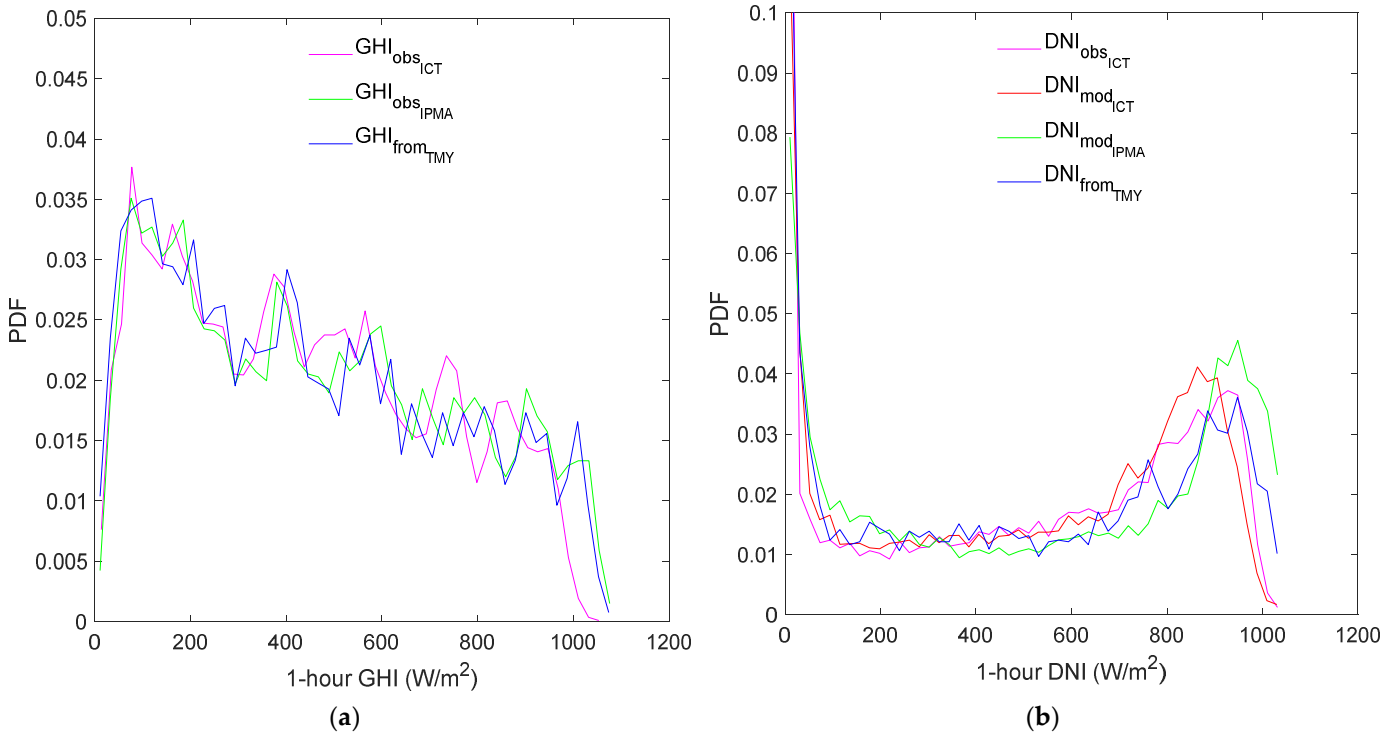

Figure 5. Probability Density Functions (PDFs) for 3 years (2017–2019) and for TMY: (**a**) GHI observed at ICT, IPMA stations and calculated from TMY, using IPMA data; (**b**) DNI observed and modelled at ICT station, DNI modelled at IPMA stations and calculated from TMY, using IPMA data.

3.4. IPMA's Main Stations: DNI Availabilities and CF Estimations

Considering IPMA's main stations, the results of DNI availability (estimated from TMY) are presented in Table 4, where stations are ordered by location, i.e., from the southernmost station to the northernmost one. Additional details regarding all IPMA network stations will be discussed in the next subsection (Section 3.5). By analysing the data presented in Table 4, it is possible to notice that the highest annual DNI and GHI availabilities are verified at Faro and Sagres stations (coastal Southern Portugal) with 2280.66 and 1988.94 kWh/m²/year, respectively. In contrast, the smallest DNI and GHI availability values were obtained at Penhas Douradas (interior central Eastern Portugal) and Cabo Carvoeiro (coastal central Western Portugal), with 1521.87 and 1625.36 kWh/m²/year, respectively.

Table 4. Estimated DNI availability, GHI availability, and capacity factor (CF), from IPMA data (IPMA main stations).

Station Names	E_b (kWh/m²/year)	E_g (kWh/m²/year)	CF (%)
Sagres	2245.30	1988.94	35.2
Faro	2280.66	1963.54	36.2
Sines	2024.39	1854.89	31.9
Beja	2145.45	1878.65	31.8
Évora	2030.14	1808.25	30.3
Lisboa/Geofísico	1888.81	1755.44	29.1
Lisboa/Gago Coutinho	1985.18	1788.31	30.1
Portalegre	1875.37	1698.47	27.4
Cabo Carvoeiro	1521.87	1625.36	22.8
Castelo Branco	2078.07	1769.59	31.2
Coimbra	1809.43	1645.21	25.7
Penhas Douradas	1467.85	1672.30	19.4
Viseu	1786.90	1622.90	26.1
Porto	1624.47	1603.49	24.2
Vila Real	1603.01	1561.46	23.6
Bragança	1847.01	1648.14	28.3

At Faro, DNI availabilities of ~2280.66 kWh/m²/year are obtained, while observed GHI availabilities are found to be ~1963.54 kWh/m²/year. At Sines, the modelled DNI availability is ~2024.39 kWh/m²/year, where GHI availability values are ~1854.89 kWh/m²/year. In Cavaco et al. [8], DNI average availability was calculated for Sines from 4 years of measured data, having obtained a value of ~2081 kWh/m²/year. This represents a relative difference of ~2.72%. At Évora, an availability value of ~2030.14 kWh/m²/year was obtained for the modelled DNI and ~1808.25 kWh/m²/year for observed GHI. Considering an average DNI availability for the 4 years of measured data used in the model validation, a value of ~2076.80 kWh/m²/year is found. The difference in annual availability of measured and modelled DNI is ~2.25%, which shows good agreement between the two. Stations at Lisboa/Geofísico and Lisboa/Gago Coutinho (~5.6 km apart) show DNI availabilities of ~1888.81 and 1985.18 kWh/m²/year, respectively, while respective GHI availabilities are found to be ~1755.44 and 1788.31 kWh/m²/year. An average availability of DNI and GHI from 5 years of ground-based measurements at Lisboa/LNEG was found to be ~1918 and 1715 kWh/m²/year, respectively, as shown in Cavaco et al. [8]. The Lisboa/LNEG station is located ~4.4 km from Lisboa/Gago Coutinho station, where differences in DNI and GHI availability between these stations are about ~3.50 and 4.27%, respectively. The high DNI availability value at the Lisboa/Gago Coutinho station is directly related to the high GHI availability value obtained at this station, comparing with the values measured at Lisboa/LNEG. It can be concluded that

for the main IPMA stations located in the southern region of Portugal, the modelled DNI availabilities are in good agreement with those presented in Cavaco et al. [8] from observed data. Considering DNI availability obtained in Cabo Carvoeiro, located in interior central western Portugal, a value of ~1521.87 kWh/m²/year is found for the model. The value obtained by the model is relatively low, considering that the availability of GHI measured is ~1625.36 kWh/m²/year. It should be mentioned that GHI measurements at this station started in August 2002, with an interruption during February 2006. In this case, measurements were restarted in November 2007, where measured values were shown to be relatively higher. Furthermore, Santa Cruz (a secondary station) is ~26 km from Cabo Carvoeiro, where DNI and GHI availabilities of ~1889.36 and ~1703.69 kWh/m²/year can be found, respectively. The disagreement between values for Cabo Carvoeiro and Santa Cruz may point to a poor DNI estimation at Cabo Carvoeiro, which may result from a poor source of quality data for GHI, thus contributing to a lower performance of the model output. At Castelo Branco, the DNI and GHI availabilities are ~2078.07 and ~1769.59 kWh/m²/year, respectively. Castelo Branco is a station located in the interior in the central eastern region of Portugal. Penhas Douradas station has DNI and GHI availability values of ~1467.85 and 1672.30 kWh/m²/year, respectively. The Aldeia Souto (secondary) station is located about 16 km east of Penhas Douradas, where it is possible to observe DNI and GHI availabilities of ~1825 and 1648 kWh/m²/year, respectively. The Covilhã (secondary) station is located about 18 km south of Penhas Douradas, where availabilities of ~2091 and 1739 kWh/m²/year for DNI and GHI are found, respectively. This seems to point to the fact that DNI estimations for Penhas Douradas station are anomalously low for that region. Still, this station is part of the Serra da Estrela natural park, and can be affected by local weather effects like the formation of clouds. At Porto, the DNI availability obtained with the model is ~1624.47 kWh/m²/year and the GHI availability is ~1603.49 kWh/m²/year. At Porto/S. gens, a secondary station that is at a distance of about 6 km from Porto station, the DNI and GHI availability is found to be ~1630.00 and ~1543.47 kWh/m²/year. Both values are consistent and reveal lower levels of solar radiation in this region (i.e., in the northern part of the country and on the coast). Finally, at Bragança, the DNI and GHI availabilities are found to be ~1847.01 and ~1648.14 kWh/m²/year, respectively.

In Table 4, CF values (estimated from the SAM) for the main IPMA stations are presented. CF values higher than 30% are considered as benchmark values for the installation of CSP plants in a region of interest. Such a benchmark comes naturally from the fact that stations with higher CF have higher production capabilities, making them more suitable for bankable CSP projects. In this regard, the Faro station, which is a station located in a coastal area in the southeastern region of the country, depicts a CF of ~36.2%. This is the highest value for Portugal, making it a region of particular interest for the implementation of CSP power plants. Moreover, Sines is located in the southwestern coastal region, with a CF value of ~31.9%. Regarding the CF value at Évora, ~30.3% is obtained. CF values of ~29.1 and 30.1% are obtained at Lisboa/Geofísico and Lisboa/Gago Coutinho, respectively. Both these stations are in the southwestern region of Portugal. CF values of ~22.8% are found at Cabo Carvoeiro. This low value results from the low DNI availabilities estimated for this region, as previously mentioned. As a matter of fact, the CF value from Santa Cruz station (~28%), being located about 26 km away from Cabo Carvoeiro, tends to indicate that the value for Cabo Carvoeiro is anomalously low. At Castelo Branco, a CF of ~31.2% is obtained, while in Penhas Douradas station the CF is found to be ~19.4%, which is directly related to the low value of DNI availability, as previously discussed. Stations like Aldeia Souto and Covilhã, located ~16 and 18 km away from Penhas Douradas, have CF values of ~26.9 and 30.6%, respectively. The CF values calculated at Porto and Porto/S. gens were ~24.2 and 23.7%, respectively, while Bragança (located in the northeastern region) shows a CF of ~28.3%.

3.5. PMA Network: Assessment of Solar Availability

In Table A1 of Appendix A, a summary can be found for the DNI and GHI availabilities, and for the CF, found for all the stations within the IPMA network. Regarding DNI and GHI availabilities, it is possible to find DNI values between ~1263 kWh/m²/year at Montalegre in the interior northwestern, and ~2310 kWh/m²/year at Castro Marim in the interior southeastern. Regarding GHI availabilities, the values range between ~1383 kWh/m²/year at Montalegre in the interior northwestern area, and ~1989 kWh/m²/year at Sagres in the coastal southwestern area, the southernmost station of the IPMA network. In fact, there is a clear tendency for the increase of DNI and GHI from north to south and from west to east, as further discussed.

In Figure 6a, a GHI availability map is shown, being calculated from the TMY with the observed values. Considering observed GHI availability, the southern region of Portugal depicts higher values. These range from ~1725 kWh/m²/year in Viana do Alentejo to ~1989 kWh/m²/year in Sagres. In the eastern region, values range between ~1650 and 1780 kWh/m²/year. In the north and west, values range between ~1383 and 1700 kWh/m²/year. Similar ranges of GHI availability values can be found in ref. [46]. For the case of DNI availability maps with values estimated from IPMA data, presented in Figure 6b, in the southern region with the most sun exposure, values range between ~1800 and 2310 kWh/m²/year. More to the eastern side, in the Beira Interior region, values range between ~1400 and 2100 kWh/m²/year. Regarding the northern area, values range between ~1200 and 1847 kWh/m²/year. In the western area, values of annual DNI availability ranging between ~1400 and ~1900 kWh/m²/year can be found. These large ranges of values for the estimated DNI availability within the same region are a consequence of observed GHI spatial variation, which may be affected by local meteorological conditions of the areas where the stations are located or by errors that may result from measuring inaccuracies. It is worth noting the DNI availability values above 2000 kWh/m²/year in the interior central eastern region of Portugal (Beira Interior region). Beira Interior has very particular climatic nuances, with cold to very cold winters and moderate to very hot summers [47].

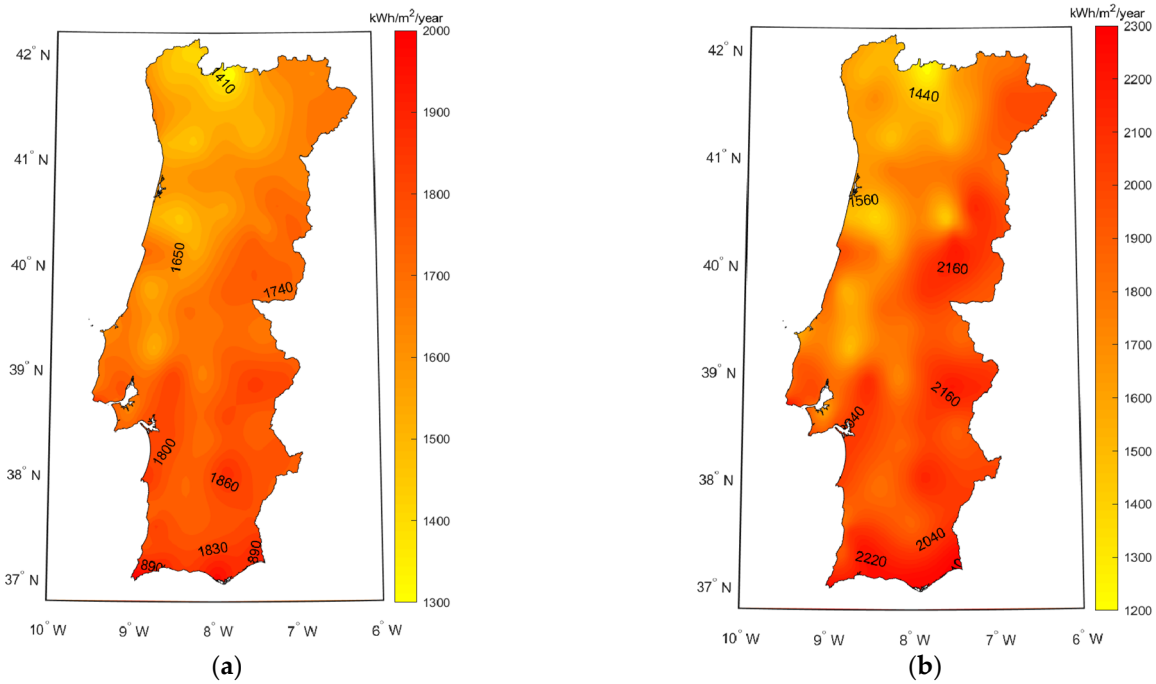

Figure 6. Availability maps (kWh/m²/year) calculated from the TMY (%) estimated from IPMA stations: (**a**) GHI, (**b**) DNI.

3.6. IPMA Network: Production Capacity of CSP Plants

In this work, a case study is considered focusing an operational CSP facility with a similar configuration to Andasol3. Figure 7 shows the Andasol3 solar power plant. Finally, regarding the obtained CF, illustrated in Figure 8, values range between ~17.8%, at Montalegre in the northwest, and 36.2%, at Faro. There is a general increase from north to the south and from west to east in Portugal, following the previously shown DNI and GHI availability values, as expected. Chaves station is 29 km from Montalegre and a CF value of 23.2% was found. The low CF value in Montalegre is directly related to the local GHI measurement. It is also worth mentioning that the CF value in Penhas Douradas, 19.4%, is low compared to other stations in the Beira Interior region (e.g., Covilhã, 30.6%). Anomalies have already been identified in the GHI measurements at Penhas Douradas and this is reflected in the DNI estimation and, consequently, in the CF value. The regions of Beira Interior (that includes the Castelo Branco and Covilhã stations), Alentejo (a region on the South of Portugal that encompasses Portalegre, Sines, Évora and Beja stations), and Algarve (southernmost region that comprises Sagres and Faro), which had already been highlighted by its DNI availability values, shows high CF levels, reaching values higher than 30%.

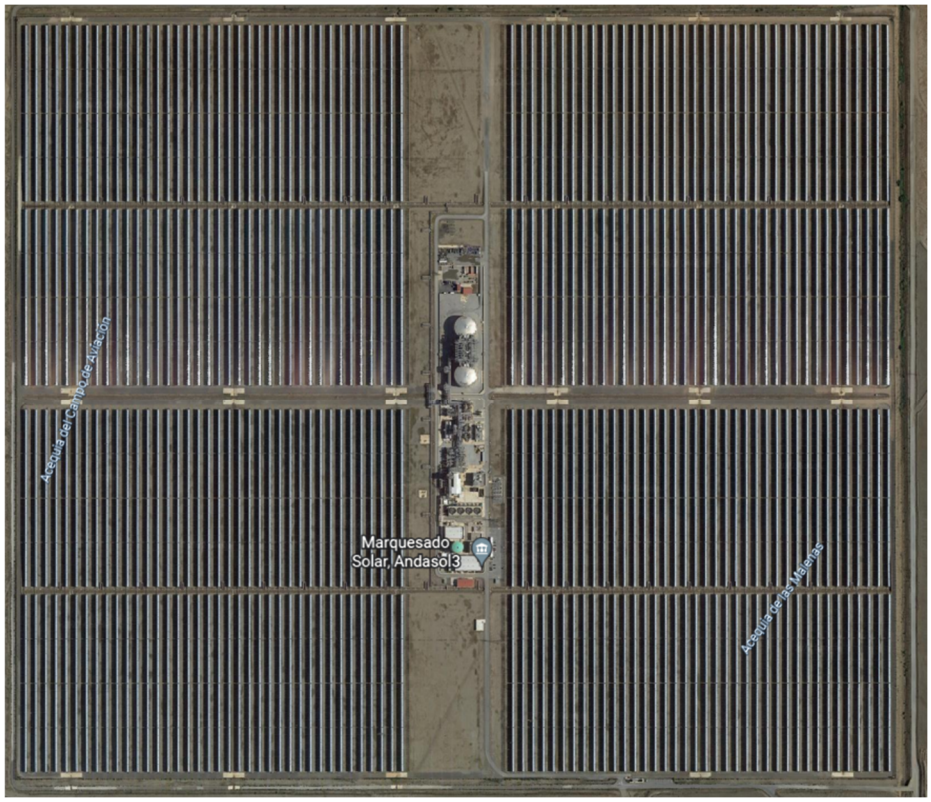

Figure 7. Andasol3 power plant located in Aldeire (Granada, Spain). All rights reserved to © Google Earth.

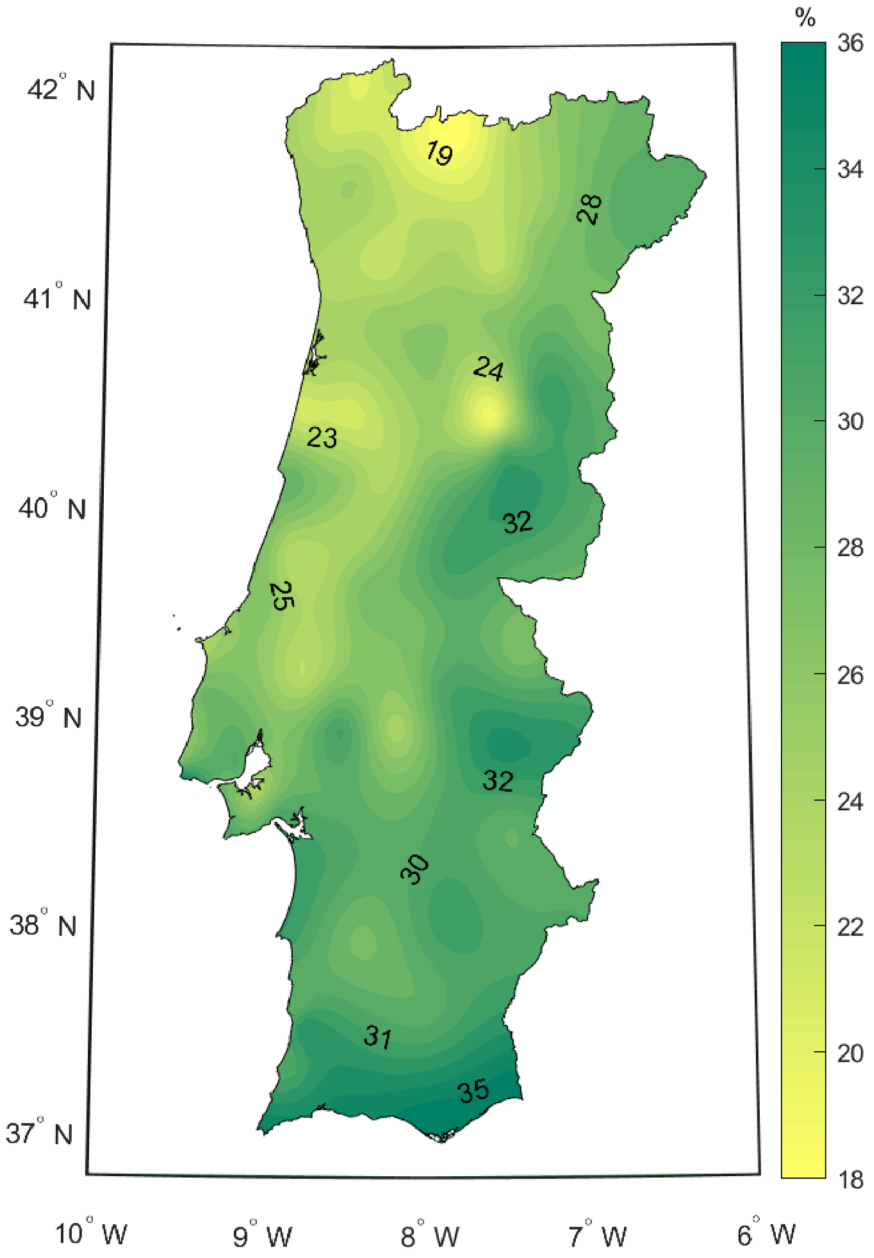

Figure 8. Capacity factor (CF) map for continental Portugal calculated from the TMY meteorological data obtained through the IPMA stations.

4. Implications for Decision Making

It is worth noting that Portugal has a national plan for energy and climate (*Roteiro para a Neutralidade Carbono*—RNC2050, as proposed through the European Commission [48]) towards carbon neutrality until 2050. The plan sets an ambitious target that aims at a strong implementation of renewable energies in the energy sector to reach an energy mix with almost exclusively renewables. According to this document, CSP should act as an anchor for the irregularity of wind and PV, the latter only being produced during the day. This is because cheap storage is achievable for CSP technologies, allowing the storage to be sized in such way as to produce energy for almost 24 h a day. Additionally, CSP can be hybridized with PV such that PV produces energy during the day with no storage and CSP stores energy during the day for night use. Furthermore, in the Portuguese energy sector, one of the largest contributions of renewables comes from hydroelectric plants, 23% of the total 59% in 2021 [49], which is lower during summer months and will tend to

decrease if the tendency for a reduction in precipitation is confirmed in the future. Thus, the implementation of CSP technology in Portugal, as shown in this study, can be complementary to other renewable sources, providing its contribution to reach important objectives of the RNC2050. The present work provides concrete indications for regions of great interest for the installation of CSP systems, such as Beira Interior, Alentejo, and Algarve. This contribution is based on the availability values of DNI, and CF, presented in this analysis. It is planned that a more in-depth study, to be carried out in the future, will enable the introduction of other factors, such as proximity to the electric grid, road access, and soiling, that influence the feasibility of the project.

In such a context, according to the report published by National Energy Grids (*Redes Energéticas Nacionais*—REN), in 2021 the power consumption of Portugal was ~49.5 TWh, from which 59% was produced by renewable energy [49]. This means that, to reach the goals of RNC2050, the remaining 41% of energy must be produced by renewable sources before 2050. Thus, to have an idea of how CSP could contribute to that objective, let us assume a hypothetical scenario that all this energy is produced from CSP plants installed in the most suitable region of Portugal; according to CF values, that is Faro; this means that approximately 128 plants like Andasol3 would have to be deployed in this region, occupying an area of ~65.3 km^2. In fact, the actual number of CSP plants in Spain is roughly 51, this means that the hypothetical scenario would have 2.51 times more CSP power plants than the number of plants already operating in Spain now. This reveals that such a scenario for a 100% renewable energy mix, may be difficult to reach, but it is not definitely unreachable, especially if new technologies like direct molten-salt CSP plants [30,50] reach the market development with higher efficiencies at lower level energy costs.

5. Conclusions

In this work, an evaluation concerning the production capacity of CSP plants is carried out by estimating CF values. The CF assessment is performed using the SAM software, which requires as input meteorological variables. The main one being DNI, which was modelled from a GHI, measured in a national meteorological network, using the Engerer2 model and MRM, both evaluated and calibrated for a benchmark station located at Évora (Southern Portugal). Additionally, DNI availability maps based on the regional TMY were also produced at different ground stations. The TMY were further used in simulations of an Andasol3-like power plant. From such simulations, CF values were obtained. In summary, the main conclusions of this work can be stated as follows:

- DNI values modelled from GHI with the use of Engerer2 show very good agreement with the observations;
- GHI and DNI annual availabilities estimated for the IPMA network show very good accordance with previous values found in the literature;
- Annual DNI availabilities and CFs were found to be as high as ~2310 kWh/m^2 and ~36.2% in Castro Marim and in Faro cities in Algarve, respectively.
- DNI availability and CF mapping showed the existence of three preferential regions for CSP installation: two in Southern Portugal—Alentejo and Algarve regions; and one in eastern central Portugal—Beira Interior region);

A more detailed regional study is planned, which should include the information of other factors, such as proximity to the electric grid, road access, and soiling. Finally, it is important to highlight that the method used in this work is not restricted to Portugal, and can be applied, as a tool to support decision making at similar regions worldwide that have a high potential for CSP.

Author Contributions: The concept of this work was formed by A.M.T., R.C., F.M.L. and H.G.S. The applied methodology was implemented by A.M.T., R.C., F.M.L. and H.G.S. The use of the SAM software was carried out by A.M.T. and F.M.L. Analysis, validation, investigation, resources, data curation were made by A.M.T. The original draft preparation was written and editing by A.M.T. and H.G.S. All authors have read and agreed to the published version of the manuscript.

Funding: This work is supported by national funding awarded by FCT—Foundation for Science and Technology, I.P., projects ICT—UIDB/04683/2020 and LAETA—UIDB/50022/2020. A.M. Tavares acknowledges the PhD grants *Programa de Bolsas CAMÕES I.P./MILLENNIUM.* F.M. Lopes acknowledges FCiênciasID for the postdoctoral research grants (PTDC/CTA-MET/28946/2017 and H2020-IBA-SPACE-CHE2-2019—reference 958927). R. Conceição acknowledges the European Union's Horizon 2020 research and innovation programme under grant agreement N° 823802 (SFERA-III) and wishes to thank to "Comunidad de Madrid" and European Structural Funds for their financial support to ACES2030-CM project (S2018/EMT-4319). H.G. Silva acknowledges the Physics Department of the University of Évora for supporting his work.

Institutional Review Board Statement: Not applicable.

Informed Consent Statement: Not applicable.

Acknowledgments: A.M. Tavares ICT to provide good working conditions and for making available the solar irradiance data. F.M. Lopes acknowledges IDL and IPMA. Finally, the authors are grateful to: Thomas Fasquelle for the development of SAM's Andasol 3 script; IPMA, particularly to Jorge Neto, for providing the meteorological data; P. Canhoto and E. Abreu, for the maintenance of solar radiation measurements at the ICT station in Évora.

Conflicts of Interest: The authors declare no conflict of interest.

Nomenclature

β_n	Coefficients of Engerer model
ΔE_b	Relative difference of DNI availability [%]
Δk_{tc}	Deviation between the observed value of k_t at surface and the one obtained under clear sky [dimensionless]
σ	standard deviation
AST	Apparent solar time [h]
C	Lower asymptote [dimensionless]
CF	Capacity factor [%]
DHI	Diffuse Horizontal Irradiance [W/m²]
DNI	Direct Normal Irradiance [W/m²]
DNI_{cs}	Direct Normal Irradiance at clear-sky [W/m²]
GHI	Global Horizontal Irradiance [W/m²]
GHI_{cs}	Global Horizontal Irradiance at clear-sky [W/m²]
DNI_i^{ADJ}	adjusted modelled DNI [W/m²]
E_b	DNI availability [kWh/m2/year]
E_g	GHI availability [kWh/m2/year]
Elev	Elevation of each station [m]
E_{0n}	Irradiance at the top of the atmosphere
K	diffuse fraction [dimensionless]
k_e	portion of K attributed in case of cloud enhancement [dimensionless]
k_t	Clearness index [dimensionless]
k_{tc}	Clearness index at clear-sky [dimensionless]
MAE	Mean Absolute Error [W/m²]
MBE	Mean Bias Error [W/m²]
P	Atmospheric pressure [hPa]
$Prec$	Precipitation [mm]
r	correlation coefficient [dimensionless]
R^2	coefficient of determination [dimensionless]
RH	Relative Humidity [%]
RMSE	Root Mean Square Error [W/m²]
T_a	Ambient Temperature [°C]
WS	Wind Speed [m/s]
Z	Zenith angle [°]
CDF	Cumulative Frequency Distribution Function
CSP	Concentrating Solar Power
FS	Finkelstein-Schafer statistic
IPMA	Instituto Português do Mar e da Atmosfera
MRM	Multivariate Regression Model

SAM	System Advisor model
TMM	Typical Meteorological Month
TMY	Typical Meteorological Year

Appendix A

Table A1. List of all IPMA stations (latitude, longitude, elevation, years of available data, annual DNI and GHI availabilities, capacity factor, and annual power generation).

Station Names	Latitude (°N)	Longitude (°W)	Elevation (m)	Period of Data (Years)	E_b (kWh/m²/year)	E_g (kWh/m²/year)	CF (%)	Annual Power Generation (GWh/year)
Cabo Carvoeiro/Farol	39.36	−9.41	32.00	9.01	1521.87	1625.36	22.8	99.79
Sagres/Quartel da Marinha	37.01	−8.95	22.85	10.02	2245.30	1988.94	35.2	154.35
Lisboa/Geofísico	38.72	−9.15	77.00	13.30	1888.81	1755.44	29.1	127.50
Sines/Monte Chãos	37.95	−8.84	103.00	19.72	2024.39	1854.89	31.9	139.87
Viana do Castelo/Meadela	41.71	−8.80	16.00	4.79	-	-	-	-
Porto/Pedras Rubras	41.23	−8.68	69.00	17.63	1624.47	1603.49	24.2	105.95
Coimbra/Aeródromo	40.16	−8.47	171.00	17.01	1809.43	1645.21	25.7	112.64
Faro/Aeroporto	37.02	−7.97	5.00	16.96	2280.66	1963.54	36.2	158.71
Évora/Aeródromo	38.54	−7.89	247.56	13.21	2030.14	1808.25	30.3	132.53
Viseu/Aeródromo	40.71	−7.90	644.37	13.97	1786.90	1622.90	26.1	114.49
Beja	38.03	−7.87	246.00	17.02	2145.45	1878.65	31.8	139.48
Vila Real/Aeródromo	41.27	−7.72	561.00	19.92	1603.01	1561.46	23.6	103.28
Penhas Douradas/Observatório	40.41	−7.56	1380.00	14.80	1467.85	1672.30	19.4	84.98
Castelo Branco	39.84	−7.48	386.00	11.83	2078.07	1769.59	31.2	136.84
Portalegre	39.29	−7.42	597.00	17.07	1875.37	1698.47	27.4	120.20
Bragança	41.80	−6.74	690.00	17.57	1847.01	1648.14	28.3	123.87
Lisboa/Gago Coutinho	38.77	−9.13	103.88	17.14	1985.18	1788.31	30.1	131.73
Odemira/S. Teotónio	37.55	−8.73	120.54	15.92	2051.54	1825.73	32.4	141.95

Vila Nova de Cerveira/Aeródromo	41.97	−8.68	34.00	15.30	1618.96	1532.58	23	100.88
Monção/Valinha	42.07	−8.38	80.00	15.14	1555.61	1466.69	20.6	90.43
Lamas de Mouro	42.04	−8.20	880.00	15.12	1553.14	1464.82	22.5	98.48
Montalegre	41.82	−7.79	1005.00	15.78	1262.83	1383.36	17.8	77.85
Ponte de Lima/Escola Agrícola	41.76	−8.57	40.00	17.20	1538.06	1518.47	22.1	97.01
Chaves/Aeródromo	41.73	−7.47	360.00	17.97	1627.84	1568.18	23.2	101.46
Cabril/S. Lourenço	41.71	−8.03	585.00	6.70	1460.30	1458.28	19.9	87.27
Braga/Merelim	41.58	−8.45	68.35	16.30	1725.64	1571.64	25.1	109.81
Cabeceiras de Basto	41.49	−7.98	350.00	16.99	1549.57	1521.93	22.3	97.81
Mirandela	41.51	−7.19	250.00	13.33	1704.56	1597.46	25.3	110.66
Macedo de Cavaleiros/Izeda-Morais	41.57	−6.79	702.00	13.51	1991.53	1679.19	29	126.92
Miranda do Douro	41.50	−6.27	693.00	12.72	1992.55	1709.17	29.2	127.86
Mogadouro	41.34	−6.73	644.00	17.08	1973.36	1685.47	29.3	128.30
Carrazêda de Ansiães	41.24	−7.30	715.00	16.97	1665.29	1574.04	26	113.84
Porto/S.Gens	41.18	−8.64	89.19	6.81	1630.00	1543.47	23.7	103.68
Moncorvo	41.19	−7.02	600.00	17.04	1889.45	1662.77	27.8	121.68
Pinhão	41.17	−7.55	130.00	9.92	1508.15	1535.83	22	96.52
Luzim	41.15	−8.25	287.17	9.39	1510.18	1492.18	22.3	97.71
Moimenta da Beira	40.99	−7.60	715.00	16.80	1776.39	1633.02	25.7	112.72
Trancoso/Bandarra	40.78	−7.35	840.00	15.89	1931.57	1692.99	28.6	125.06
Arouca	40.93	−8.26	270.00	5.88	1775.57	1612.02	25.5	111.64
Figueira de Castelo Rodrigo/V.Torpim	40.83	−6.94	635.00	16.23	1843.46	1653.39	27.5	120.40
Guarda	40.53	−7.28	1020.00	16.13	2111.23	1734.55	31.1	136.01
Nelas	40.52	−7.86	425.00	16.07	1745.60	1580.33	25.3	110.88
Pampilhosa da Serra	40.15	−7.93	835.59	13.55	1918.11	1664.43	27.5	120.49
Covilhã	40.26	−7.48	482.00	14.41	2090.86	1738.84	30.6	133.96
Aldeia Souto/Quinta Lageosa	40.35	−7.39	468.00	7.93	1824.67	1647.52	26.9	117.68

Lousã/Aeródromo	40.14	−8.24	193.77	11.85	1608.49	1555.31	23.4	102.40
Aveiro/Universidade	40.64	−8.66	5.00	17.79	1607.61	1586.50	23.7	103.92
Dunas de Mira	40.45	−8.76	14.00	7.57	1510.74	1535.10	21.3	93.42
Anadia/Estação Vitivinícola da Bairrada	40.44	−8.44	45.00	17.48	1399.34	1487.32	21.4	93.54
Coimbra/Bencanta	40.21	−8.46	35.00	10.22	1691.03	1593.23	24.7	108.26
Figueira da Foz/Vila Verde	40.14	−8.81	4.00	16.50	1963.77	1717.17	28.8	126.00
Ansião	39.90	−8.41	396.24	15.01	1721.54	1612.64	24	105.13
Leiria/Aeródromo	39.78	−8.82	45.00	11.38	1573.39	1567.91	23.2	101.81
Leiria/Barosa	39.75	−8.83	24.00	4.14	-	-	-	-
São Pedro de Moel	39.76	−9.03	40.00	9.15	1917.07	1675.57	27.3	119.62
Tomar/Vale Donas	39.59	−8.37	75.42	15.94	1860.74	1710.12	27.4	119.81
Alcobaça/Estação Fruticultura	39.55	−8.97	38.00	16.66	1781.07	1669.28	26.5	116.08
Vieira Natividade	39.31	−8.92	52.83	14.55	1692.12	1648.63	25.1	110.04
Rio Maior/ETAR	39.20	−8.74	71.91	17.04	1522.67	1554.56	22.9	100.17
Santarém	39.04	−9.18	110.00	16.05	1924.50	1726.04	28.3	123.76
Torres Vedras/Dois Portos	38.94	−8.51	18.75	16.15	2115.38	1825.18	31.2	136.68
Coruche/Estação de Regadio (INIA)	39.13	−9.38	40.71	8.81	1889.36	1703.69	28	122.52
Santa Cruz/Aeródromo	38.78	−9.50	141.23	6.68	1893.25	1695.90	26.4	115.59
Cabo da Roca	38.71	−9.18	69.96	8.90	1861.28	1722.95	27.9	122.40
Lisboa/Tapada da Ajuda	38.71	−9.49	7.88	9.63	2218.63	1847.57	34.1	149.16
Cabo Raso/Farol								

Barreiro/Lavradio	38.67	−9.05	6.00	16.04	1604.73	1649.61	23.4	102.37
Pegões	38.65	−8.64	64.00	6.80	2044.33	1810.87	28.9	126.75
Setúbal/Estação de Fruticultura	38.55	−8.89	35.00	16.06	1963.72	1769.06	29.9	130.77
Almada/Praia da Rainha	38.62	−9.21	5.51	16.63	1885.80	1743.98	28.6	125.25
Alcácer do Sal—Barrosinha	38.36	−8.48	29.00	16.49	1999.84	1801.29	30.5	133.69
Alvalade	37.95	−8.39	46.97	15.37	1838.25	1740.06	27.7	121.47
Zambujeira	37.58	−8.74	67.00	9.79	1901.81	1769.89	29.9	131.05
Aljezur	37.33	−8.80	11.95	13.79	1931.27	1787.92	30.3	132.60
Foía	37.31	−8.60	895.30	8.67	2213.31	1809.38	32.8	143.55
Sabugal/Martim Rei	40.34	−7.04	858.00	14.39	2067.15	1749.23	30.6	133.82
Zebreira	39.85	−7.07	374.00	15.48	1963.11	1742.58	29.8	130.43
Proença-a-Nova/Moitas	39.73	−7.87	379.00	14.73	2069.83	1751.58	31.1	136.19
Alvega	39.46	−8.03	51.05	15.87	1836.80	1693.62	27.6	120.75
Avis/Benavila	39.11	−7.88	152.25	16.30	1986.54	1753.16	30.6	133.97
Mora	38.94	−8.16	129.45	6.41	1730.08	1670.45	24.3	106.43
Elvas/Est. Melhoramento Plantas	38.89	−7.14	209.97	16.71	2127.34	1815.76	32.7	143.33
Estremoz/Techocas	38.86	−7.51	366.00	16.31	2198.18	1845.04	33.6	147.34
Reguengos/S.Pedro do Corval	38.48	−7.47	265.17	9.39	1905.44	1744.70	29	126.94
Viana do Alentejo	38.33	−8.05	202.00	8.66	1890.40	1724.96	29.9	130.93
Amareleja	38.21	−7.21	192.00	9.45	1996.22	1798.38	29.8	130.74
Amareleja2	38.20	−7.23	180.00	4.58	-	-	-	-
Mértola/Vale Formoso	37.76	−7.55	190.00	15.54	2044.28	1802.03	30.9	135.48
Castro Verde/Neves Corvo	37.58	−7.97	225.00	17.13	1882.23	1779.48	29.4	128.73
Castro Marim/Reserva	37.23	−7.43	4.83	16.57	2310.08	1912.79	35.6	155.96

Nacional do Sapal Porti-mão/Aeródromo	37.15	−8.58	2.00	16.19	2196.05	1882.81	34.1	149.24

Appendix B

Table A2. Hourly multivariate regression metrics obtained with the stepwise function considering a third-degree polynomial adjustment of DNI (MRM) for four years (from 2017 to 2019).

DNI Adjusted				
Terms	**Estimates**	**SE**	**tStat**	***p*Value**
(Intercept)	0	0	-	-
x_1	−4.28	2.72	−1.57	0.11
x_2	25.26	6.68	3.78	1.55×10^{-4}
x_3	6.11	5.01	1.22	0.22
x_4	1.37	0.66	2.07	0.04
x_5	−16.78	40.65	−0.41	0.68
x_6	−10.35	7.46	−1.39	0.17
x_7	−5.80	6.18	−0.94	0.35
x_8	0.13	0.15	0.81	0.42
$x_1 \times x_2$	-1.16×10^{-3}	5.53×10^{-3}	−0.21	0.83
$x_1 \times x_3$	6.62×10^{-3}	2.11×10^{-3}	3.13	1.74×10^{-3}
$x_1 \times x_4$	1.08×10^{-3}	6.29×10^{-4}	1.72	0.09
$x_1 \times x_5$	0.08	0.10	0.79	0.43
$x_1 \times x_6$	-5.37×10^{-3}	4.36×10^{-3}	−1.23	0.22
$x_1 \times x_7$	−0.02	7.71×10^{-3}	−2.51	0.01
$x_1 \times x_8$	4.16×10^{-3}	2.65×10^{-3}	1.57	0.12
$x_2 \times x_3$	−0.01	9.91×10^{-3}	−1.43	0.15
$x_2 \times x_4$	-9.85×10^{-3}	2.15×10^{-3}	−4.59	4.47×10^{-6}
$x_2 \times x_5$	−0.65691	0.134572	−4.88	1.07×10^{-6}
$x_2 \times x_6$	0.03	0.01	2.41	0.01
$x_2 \times x_7$	0.04	0.01	3.28	1.05×10^{-3}
$x_2 \times x_8$	−0.02	6.43×10^{-3}	−3.49	4.88×10^{-4}
$x_3 \times x_4$	7.81×10^{-3}	2.50×10^{-3}	3.13	1.78×10^{-3}
$x_3 \times x_5$	−0.01	0.02	−0.52	0.61
$x_3 \times x_6$	−0.12	0.03	−4.46	8.20×10^{-6}
$x_3 \times x_7$	−0.01	0.01	−0.87	0.38
$x_3 \times x_8$	-6.17×10^{-3}	4.75×10^{-3}	−1.30	0.19
$x_4 \times x_5$	0.01	0.01	0.96	0.34
$x_4 \times x_6$	0.01	6.33×10^{-3}	2.38	0.02
$x_4 \times x_7$	4.52 × 10−03	0.01	0.41	0.68
$x_5 \times x_6$	0.18	0.06	3.26	1.10×10^{-3}
$x_5 \times x_7$	0.50	0.23	2.20	0.03
$x_5 \times x_8$	4.00×10^{-3}	0.04	0.10	0.92
$x_6 \times x_8$	-2.91×10^{-3}	6.98×10^{-3}	−0.42	0.68
x_1^2	-5.81×10^{-3}	3.11×10^{-3}	−1.87	0.06
x_2^2	4.90×10^{-3}	3.23×10^{-3}	1.52	0.13
x_3^2	-1.84×10^{-3}	6.33×10^{-3}	−0.29	0.77
x_4^2	-5.21×10^{-3}	1.08×10^{-3}	−4.81	1.55×10^{-6}
x_6^2	0.15	0.03	4.70	2.66×10^{-6}

x_7^2	0.87	0.64	1.35	0.18
$x_1 \times x_2 \times x_3$	7.32×10^{-5}	8.25×10^{-6}	8.87	8.44×10^{-19}
$x_1 \times x_2 \times x_4$	-9.92×10^{-6}	1.97×10^{-6}	−5.03	5.00×10^{-7}
$x_1 \times x_2 \times x_5$	1.39×10^{-4}	3.91×10^{-5}	3.57	3.63×10^{-4}
$x_1 \times x_2 \times x_6$	1.49×10^{-5}	1.10×10^{-5}	1.36	0.17
$x_1 \times x_2 \times x_7$	-8.68×10^{-5}	4.48×10^{-5}	−1.94	0.05
$x_1 \times x_2 \times x_8$	-8.43×10^{-6}	4.68×10^{-6}	−1.80	0.07
$x_1 \times x_3 \times x_4$	-7.57×10^{-7}	2.60×10^{-6}	−0.29	0.77
$x_1 \times x_3 \times x_5$	-1.64×10^{-5}	3.42×10^{-5}	−0.48	0.63
$x_1 \times x_3 \times x_6$	1.77×10^{-5}	1.03×10^{-5}	1.73	0.08
$x_1 \times x_3 \times x_7$	8.08×10^{-5}	4.91×10^{-5}	1.64	0.10
$x_1 \times x_4 \times x_5$	-3.81×10^{-5}	1.19×10^{-5}	−3.20	0.00
$x_1 \times x_4 \times x_6$	-4.69×10^{-6}	3.70×10^{-6}	−1.27	0.20
$x_1 \times x_4 \times x_7$	-2.97×10^{-5}	1.53×10^{-5}	−1.94	0.05
$x_1 \times x_5 \times x_6$	1.63×10^{-4}	5.95×10^{-5}	2.74	0.01
$x_1 \times x_5 \times x_8$	-6.10×10^{-5}	1.02×10^{-4}	−0.60	0.55
$x_2 \times x_3 \times x_4$	-7.39×10^{-6}	4.34×10^{-6}	−1.70	0.09
$x_2 \times x_3 \times x_5$	0.000125	5.71×10^{-5}	2.19	0.03
$x_2 \times x_3 \times x_6$	5.08×10^{-5}	1.48×10^{-5}	3.42	0.00
$x_2 \times x_3 \times x_8$	1.16×10^{-5}	9.08×10^{-6}	1.27	0.20
$x_2 \times x_4 \times x_6$	-2.23×10^{-5}	9.92×10^{-6}	−2.25	0.02
$x_2 \times x_5 \times x_6$	-2.89×10^{-4}	1.69×10^{-4}	−1.71	0.09
$x_2 \times x_5 \times x_7$	2.92×10^{-4}	5.27×10^{-4}	0.55	0.58
$x_2 \times x_5 \times x_8$	6.50×10^{-4}	1.31×10^{-4}	4.95	7.59×10^{-7}
$x_3 \times x_4 \times x_5$	-3.13×10^{-5}	2.83×10^{-5}	−1.10	0.27
$x_3 \times x_4 \times x_6$	1.12×10^{-5}	1.10×10^{-5}	1.02	0.31
$x_3 \times x_5 \times x_6$	4.54×10^{-4}	1.49×10^{-4}	3.03	0.00
$x_3 \times x_5 \times x_7$	-1.57×10^{-4}	6.05×10^{-4}	−0.26	0.80
$x_3 \times x_6 \times x_8$	9.31×10^{-5}	2.44×10^{-5}	3.82	0.00
$x_4 \times x_5 \times x_6$	-4.07×10^{-4}	8.32×10^{-5}	−4.90	9.80×10^{-7}
$x_4 \times x_5 \times x_7$	-1.38×10^{-3}	4.91×10^{-4}	−2.82	4.81×10^{-3}
$x1^2 \times x2$	2.47×10^{-5}	2.21×10^{-6}	11.19	6.57×10^{-29}
$x_1^2 \times x_3$	-1.24×10^{-5}	2.28×10^{-6}	−5.43	5.64×10^{-8}
$x_1^2 \times x_4$	8.43×10^{-7}	4.61×10^{-7}	1.83	0.07
$x_1^2 \times x_5$	-4.44×10^{-5}	9.31×10^{-6}	−4.77	1.89×10^{-6}
$x_1^2 \times x_6$	-6.60×10^{-6}	2.75×10^{-6}	−2.40	0.02
$x_1^2 \times x_7$	2.02×10^{-5}	1.34×10^{-5}	1.50	0.13
$x_1^2 \times x_8$	8.80×10^{-6}	2.99×10^{-6}	2.94	3.25×10^{-3}
$x_1 \times x_2^2$	-5.43×10^{-5}	4.34×10^{-6}	−12.50	1.31×10^{-35}
$x_1 \times x_3^2$	-2.90×10^{-5}	4.64×10^{-6}	−6.25	4.25×10^{-10}
$x_1 \times x_4^2$	1.12×10^{-6}	5.84×10^{-7}	1.92	0.05
$x_1 \times x_6^2$	3.51×10^{-5}	1.92×10^{-5}	1.83	0.07
$x_2^2 \times x_3$	-2.15×10^{-5}	3.10×10^{-6}	−6.95	3.92×10^{-12}
$x_2^2 \times x_4$	1.20×10^{-5}	3.46×10^{-6}	3.46	5.42×10^{-4}
$x_2^2 \times x_5$	-1.55×10^{-4}	4.62×10^{-5}	−3.36	7.86×10^{-4}
$x_2^2 \times x_6$	-5.26×10^{-5}	1.19×10^{-5}	−4.43	9.60×10^{-6}
$x_2 \times x_3^2$	6.95×10^{-6}	1.78×10^{-6}	3.90	9.58×10^{-5}
$x_2 \times x_4^2$	7.50×10^{-6}	1.94×10^{-6}	3.86	1.14×10^{-4}
$x_2 \times x_6^2$	−0.00018	5.10×10^{-5}	−3.44	5.89×10^{-4}
$x_3^2 \times x_4$	8.26×10^{-6}	2.04×10^{-6}	4.06	4.95×10^{-5}
$x_3^2 \times x_5$	-1.78×10^{-5}	2.31×10^{-5}	−0.77	0.44

$x_3^2 \times x_6$	-1.39×10^{-5}	6.21×10^{-6}	−2.24	0.03
$x_3^2 \times x_8$	-5.75×10^{-7}	6.09×10^{-6}	−0.09	0.92
$x_3 \times x_4^2$	-1.03×10^{-5}	2.17×10^{-6}	−4.76	1.99×10^{-6}
$x_3 \times x_6^2$	1.40×10^{-4}	4.45×10^{-5}	3.14	1.69×10^{-3}
$x_4^2 \times x_5$	3.18×10^{-5}	1.75×10^{-5}	1.82	0.07
$x_4^2 \times x_6$	2.43×10^{-6}	5.02×10^{-6}	0.49	0.63
$x_4 \times x_6^2$	-7.78×10^{-5}	2.58×10^{-5}	−3.01	2.59×10^{-3}
$x_4 \times x_7^2$	1.37×10^{-3}	6.21×10^{-4}	2.21	0.03
$x_5 \times x_6^2$	-3.16×10^{-4}	3.72×10^{-4}	−0.85	0.39
x_1^3	-3.94×10^{-6}	2.91×10^{-7}	−13.53	2.04×10^{-41}
x_2^3	1.63×10^{-5}	1.92×10^{-6}	8.51	2.02×10^{-17}
x_3^3	-2.07×10^{-6}	6.28×10^{-7}	−3.30	9.78×10^{-4}
x_4^3	4.02×10^{-6}	6.93×10^{-7}	5.80	6.80×10^{-9}
x_6^3	−0.00059	0.000122	−4.87	1.15×10^{-6}
x_7^3	−0.09	0.03	−2.81	5.00×10^{-3}

References

1. Kim, C.K.; Kim, H.G.; Kang, Y.H.; Yun, C.Y.; Kim, S.Y. Probabilistic Prediction of Direct Normal Irradiance Derived from Global Horizontal Irradiance over the Korean Peninsula by Using Monte-Carlo Simulation. *Sol. Energy* **2019**, *180*, 63–74. https://doi.org/10.1016/j.solener.2019.01.030.
2. Conceicao, R.; Alami, A.; Romero, M. Soiling Effect in Solar Energy Conversion Systems : A Review. *Renew. Sustain. Energy Rev.* **2022**, *162*, 112434 https://doi.org/10.1016/j.rser.2022.112434.
3. Silva, H.G.; Abreu, E.F.M.; Lopes, F.M.; Cavaco, A.; Canhoto, P.; Neto, J.; Collares-Pereira, M. Solar Irradiation Data Processing Using Estimator MatriceS (SIMS) Validated for Portugal (Southern Europe). *Renew. Energy* **2020**, *147*, 515–528. https://doi.org/10.1016/j.renene.2019.09.009.
4. Salazar, G.; Gueymard, C.; Galdino, J.B.; de Castro Vilela, O.; Fraidenraich, N. Solar Irradiance Time Series Derived from High-Quality Measurements, Satellite-Based Models, and Reanalyses at a near-Equatorial Site in Brazil. *Renew. Sustain. Energy Rev.* **2020**, *117*, 109478. https://doi.org/10.1016/j.rser.2019.109478.
5. Aler, R.; Galván, I.M.; Ruiz-Arias, J.A.; Gueymard, C.A. Improving the Separation of Direct and Diffuse Solar Radiation Components Using Machine Learning by Gradient Boosting. *Sol. Energy* **2017**, *150*, 558–569. https://doi.org/10.1016/j.solener.2017.05.018.
6. Gueymard, C.A.; Ruiz-Arias, J.A. Extensive Worldwide Validation and Climate Sensitivity Analysis of Direct Irradiance Predictions from 1-Min Global Irradiance. *Sol. Energy* **2016**, *128*, 1–30. https://doi.org/10.1016/j.solener.2015.10.010.
7. Padovan, A.; Del Col, D.; Sabatelli, V.; Marano, D. DNI Estimation Procedures for the Assessment of Solar Radiation Availability in Concentrating Systems. *Energy Procedia* **2014**, *57*, 1140–1149. https://doi.org/10.1016/j.egypro.2014.10.100.
8. Cavaco, A.; Canhoto, P.; Collares Pereira, M. Procedures for Solar Radiation Data Gathering and Processing and Their Application to DNI Assessment in Southern Portugal. *Renew. Energy*. **2021**, *163*, 2208–2219. https://doi.org/10.1016/j.renene.2020.10.075.
9. Schroedter-Homscheidt, M.; Benedetti, A.; Killius, N. Energy Meteorology Verification of ECMWF and ECMWF/MACC's Global and Direct Irradiance Forecasts with Respect to Solar Electricity Production Forecasts. *Meteorol. Z.* **2016**, *26*, 1–19.
10. Stoffel, T.; Renné; D; Myers, D.; Wilcox, S.; Sengupta, M.; George, R.; Turchi, C. *Concentrating Solar Power: Best Practices Handbook for the Collection and Use of Solar Resource Data*; National Renewable Energy Lab. (NREL): Golden, CO, USA, 2010. Available: https://www.nrel.gov/docs/fy10osti/47465.pdf (accessed on 5 December 2020).
11. Gueymard, C.A. Parameterized transmittance model for direct beam and circumsolar spectral irradiance. *Sol. Energy* **2001**, *71*, 325–346.
12. Engerer, N.A. ScienceDirect Minute Resolution Estimates of the Diffuse Fraction of Global Irradiance for Southeastern Australia. *Sol. Energy* **2015**, *116*, 215–237. https://doi.org/10.1016/j.solener.2015.04.012.
13. Chain, C.; George, R.A.Y.; Vignola, F. A New Operational Model For Satellite-Derived Irradiances: Description and Validation. *Sol. Energy* **2003**, *73*, 307–317.
14. Hollands, K.G.T. An improved model for diffuse radiation: correction for atmospheric back-scattering. *Sol. Energy* **1987**, 233–236.
15. Starke, A.R.; Lemos, L.F.L.; Boland, J.; Cardemil, J.M.; Colle, S. Resolution of the Cloud Enhancement Problem for One-Minute Diffuse Radiation Prediction. *Renew. Energy* **2018**, *125*, 472–484. https://doi.org/10.1016/j.renene.2018.02.107.
16. Bright, J.M.; Engerer, N.A. Engerer2: Global Re-Parameterisation, Update, and Validation of an Irradiance Separation Model at Different Temporal Resolutions. *J. Renew. Sustain. Energy* **2019**, *11*, 033701. https://doi.org/10.1063/1.5097014.
17. Gueymard, C.A. REST2: High-Performance Solar Radiation Model for Cloudless-Sky Irradiance, Illuminance, and Photosynthetically Active Radiation—Validation with a Benchmark Dataset. *Sol. Energy* **2008**, *82*, 272–285.

https://doi.org/10.1016/j.solener.2007.04.008.
18. Yang, D. Estimating 1-Min Beam and Diffuse Irradiance from the Global Irradiance : A Review and an Extensive Worldwide Comparison of Latest Separation Models at 126 Stations. *Renew. Sustain. Energy Rev.* **2022**, *159*, 112195. https://doi.org/10.1016/j.rser.2022.112195.
19. Starke, A.R.; Lemos, L.F.L.; Barni, C.M.; Machado, R.D.; Cardemil, J.M.; Boland, J.; Colle, S. Assessing One-Minute Diffuse Fraction Models Based on Worldwide Climate Features. *Renew. Energy* **2021**, *177*, 700–714. https://doi.org/10.1016/j.renene.2021.05.108.
20. Abreu, E.F.M.; Canhoto, P.; Costa, M.J. Prediction of Diffuse Horizontal Irradiance Using a New Climate Zone Model. *Renew. Sustain. Energy Rev.* **2019**, *110*, 28–42. https://doi.org/https://doi.org/10.1016/j.rser.2019.04.055.
21. Paulescu, E.; Blaga, R. A Simple and Reliable Empirical Model with Two Predictors for Estimating 1-Minute Diffuse Fraction. *Sol. Energy* **2019**, *180*, 75–84. https://doi.org/http:// dx.doi.org/10.1016/j.solener.2019.01.029.
22. Every, J.P.; Li, L.; Dorrel, D.G. Köppen-Geiger Climate Classification Adjustment of the BRL Diffuse Irradiation Model for Australian Locations. *Renew. Energy* **2020**, *147*, 2453–2469. https://doi.org/https://doi.org/10.1016/j.renene.2019.09.114.
23. Yang, D. Temporal-Resolution Cascade Model for Separation of 1-Min Beam and Diffuse Irradiance. *J. Renew. Sustain. Energy* **2021**, *13*, 056101. https://doi.org/https://doi.org/10.1063/5.0067997.
24. Comissão Europeia. PLANO NACIONAL ENERGIA E CLIMA 2021–2030 (PNEC 2030). 2019. Available: https://ec.europa.eu/energy/sites/ener/files/documents/pt_final_necp_main_pt.pdf (accessed on 5 December 2020).
25. Lopes, F.M.; Conceição, R.; Silva, H.G.; Salgado, R.; Collares-Pereira, M. Improved ECMWF Forecasts of Direct Normal Irradiance: A Tool for Better Operational Strategies in Concentrating Solar Power Plants. *Renew. Energy* **2021**, *163*, 755–771. https://doi.org/10.1016/j.renene.2020.08.140.
26. Kambezidis, H.D.; Psiloglou, B.E.; Kaskaoutis, D.G.; Karagiannis, D.; Petrinoli, K.; Gavriil, A.; Kavadias, K. Generation of Typical Meteorological Years for 33 Locations in Greece: Adaptation to the Needs of Various Applications. *Theor. Appl. Climatol.* **2020**, *141*, 1313–1330. https://doi.org/10.1007/s00704-020-03264-7.
27. Nielsen, K.P.; Vignola, F.; Ramírez, L.; Blanc, P.; Meyer, R.; Blanco, M. Excerpts from the Report: "BeyondTMY—Meteorological Data Sets for CSP/STE Performance Simulations." *AIP Conf. Proc.* **2017**, *1850*, 140017. https://doi.org/10.1063/1.4984525.
28. Hall, I.J.; Prairie, R.R.; Anderson, H.E.; Boes, E.C. Generation of a Typical Meteorological Year. In Proceedings of the 1978 Annual Meeting of the American Section of the International Solar Energy Society, Denver, CO, USA, 28–31 August 1978; pp. 669–671.
29. Conceição, R.; Lopes, F.M.; Tavares, A.; Lopes, D. Soiling Effect in Second-Surface CSP Mirror and Improved Cleaning Strategies. *Renew. Energy* **2020**, *158*, 103–113. https://doi.org/10.1016/j.renene.2020.05.054.
30. Lopes, T.; Fasquelle, T.; Silva, H.G. Pressure Drops, Heat Transfer Coefficient, Costs and Power Block Design for Direct Storage Parabolic Trough Power Plants Running Molten Salts. *Renew. Energy* **2021**, *163*, 530–543. https://doi.org/10.1016/j.renene.2020.07.110.
31. Blair, N.; Dobos, A.P.; Freeman, J.; Neises, T.; Wagner, M.; Ferguson, T.; Gilman, P.; Janzou, S. *System Advisor Model, Sam 2014.1. 14: General Description*; NREL Rep. No. TP-6A20-61019; Natl. Renew. Energy Lab.: Golden, CO, USA, 2014; Volume 13. https://doi.org/10.2172/1126294.
32. National Renewable Energy Laboratory, "Andasol 3 CSP Project," 2021. https://solarpaces.nrel.gov/project/andasol-3 (accessed 16 June 2022).
33. Instituto Português do Mar e da Atmosfera. Glossário Climatológico/Meteorológico. Available online: https://www.ipma.pt/pt/educativa/glossario/meteorologico/index.jsp?page=glossario_ef.xml&print=true (accessed on 2 August 2021).
34. *ISO 9060:1990*; Solar Energy—Specification and Classifications of Instruments for Measuring Hemispherical Solar and Direct Solar Radiation, International Organization for Standardization. Available online: www.iso.org/standard/16629.html (accessed on 5 December 2020).
35. Alami, A.; Conceiç, R.; Gonçalves, H.; Ghennioui, A. CSP Performance and Yield Analysis Including Soiling Measurements for Morocco and Portugal. *Renew. Energy* **2020**, *162*, 1777–1792. https://doi.org/10.1016/j.renene.2020.10.014.
36. Lopes, D.; Conceição, R.; Gonçalves, H.; Aranzabe, E.; Pérez, G.; Collares-pereira, M. Anti-Soiling Coating Performance Assessment on the Reduction of Soiling Effect in Second-Surface Solar Mirror. *Sol. Energy* **2019**, *194*, 478–484. https://doi.org/10.1016/j.solener.2019.10.059.
37. *ISO 9059:1990*; Solar Energy—Calibration of Field Pyrheliometers by Comparison to a Reference Pyrheliometer, International Organization for Standardization, 2014. Available online: www.iso.org/standard/16628.html (accessed on 5 December 2020).
38. Instituto Português do Mar e da Atmosfera. Rede de Estações Meteorológicas. Available online: https://www.ipma.pt/pt/otempo/obs.superficie/ (accessed on 2 August 2021).
39. Instituto Português do Mar e da Atmosfera. Parques Meteorológicos e Equipamentos. Available online: https://www.ipma.pt/pt/educativa/observar.tempo/index.jsp?page=ema.index.xml (accessed on 2 August 2021).
40. Long, C.N.; Dutton, E.G. BSRN Global Network Recommended QC Tests, V2.0. Available online: https://bsrn.awi.de/fileadmin/user_upload/bsrn.awi.de/Publications/BSRN_recommended_QC_tests_V2.pdf (accessed on 5 December 2020).
41. Kalogirou, S.A. Environmental Characteristics. In *Solar Energy Engineering: Processes and Systems*; Elsevier: Amsterdam, The Netherlands, 2014; pp. 51–92.

42. Lopes, F.M.; Silva, H.G.; Salgado, R.; Cavaco, A.; Canhoto, P.; Collares-Pereira, M. Short-Term Forecasts of GHI and DNI for Solar Energy Systems Operation: Assessment of the ECMWF Integrated Forecasting System in Southern Portugal. *Sol. Energy* **2018**, *170*, 14–30. https://doi.org/10.1016/j.solener.2018.05.039.
43. Finkelstein, J.M.; Schafer, R.E. Improved Goodness-of-Fit Tests. *Biometrika* **1971**, *58*, 641–645.
44. Lopes, F.M.; Conceição, R.; Fasquelle, T.; Silva, H.G.; Salgado, R.; Canhoto, P.; Collares-Pereira, M. Predicted Direct Solar Radiation (ECMWF) for Optimized Operational Strategies of Linear Focus Parabolic-Trough Systems. *Renew. Energy* **2020**, *151*, 378–391. https://doi.org/10.1016/j.renene.2019.11.020.
45. Instituto Português do Mar e da Atmosfera. Clima de Portugal Continental. Available online: https://www.ipma.pt/pt/educativa/tempo.clima/ (accessed on 3 August 2021).
46. Cavaco, A.; Silva, H.; Canhoto, P.; Neves, S.; Neto, J.; Pereira, M.C. Global Solar Radiation in Portugal and its variability, monthly and yearly. In WES 2016—Workshop on Earth Sciences, Institute of Earth Sciences. 2016; pp. 1–4. Available: https://dspace.uevora.pt/rdpc/bitstream/10174/19395/1/Afonso_Cavaco_et_al_WES_2016_paper_28.pdf (accessed on 3 August 2021).
47. Cunha, L. A Beira Interior—Portugal: Caracterização Física. Rota da Lã Translana percursos e marcas um Territ. Front. Beira Inter. (Portugal), Comarc. Tajo-Salor-Almonte 2008; pp. 47–53. Available online: https://www.researchgate.net/publication/324089073_A_beira_Interior_-_Portugal_caracterizacao_fisica (accessed on 3 August 2021).
48. Governo Português. Roteiro para a Neutralidade Carbónica 2050. 2019. Available online: https://www.portugal.gov.pt/download-ficheiros/ficheiro.aspx?v=%3D%3DBAAAAB%2BLCAAAAAAABACzMDexAAAut9emBAAAAA%3D%3D.Governo
49. Redes Energéticas Nacionais. DADOS TÉCNICOS. 2021. Available online: https://datahub.ren.pt/media/hkkdskwq/dados-técnicos-2021.pdf (accessed on 3 August 2021).
50. Lopes, T.; Fasquelle, T.; Silva, H.G.; Schmitz, K. HPS2—Demonstration of Molten-Salt in Parabolic Trough Plants—Simulation Results from System Advisor Model. *AIP Conf. Proc.* **2020**, *2303*, 110003. https://doi.org/10.1063/5.0031276.